THE PERFORMANCE OF QUADRILATERAL ELEMENT WITH ROTATIONAL DEGREES OF FREEDOM IN STATICS AND DYNAMICS ANALYSIS AND OPTIMIZATION

by

XINGZHI WANG

THESIS

Submitted in partial fulfillment of the requirements
for the degree of Master of Science in Aerospace Engineering at
The University of Texas at Arlington
May, 2018

Arlington, Texas

Supervising Committee:

Bo P. Wang, Supervising Professor
Kent L. Lawrence
Cheng Luo

Abstract

THE PERFORMANCE OF QUADRILATERAL ELEMENT WITH ROTATIONAL DEGREES OF FREEDOM IN STATICS AND DYNAMICS ANALYSIS AND OPTIMIZATION

Xingzhi Wang, MS

The University of Texas at Arlington, 2018

Supervising Professor: Bo P. Wang

Finite Element Method (FEM) is widely used in structural analysis, and the standard approach to increase the accuracy of analysis is increasing the total degrees of freedom (DOFs), namely, refine the mesh. By introducing the rotational DOFs, better accuracy can be achieved without change the mesh. The objective of this study was to investigate the performance of elements with rotational DOFs in statics and dynamics analysis and applying these elements to optimization. The implementation of three representative elements with rotational DOFs for statics analysis is reproduced. Also, this work implements these elements to dynamics analysis and optimization. The results show the performance of elements with rotational DOFs is better than the regular element in both statics and dynamics analysis.

Acknowledgments

Above all, I would like to thank my advisor, Prof. Bo P. Wang, for his support and help during the process of completing this work.

I express my thanks to rest of my committee members: Prof. Kent L. Lawrence and Prof. Cheng Luo for their advice.

I would also like to thank the Department of Mechanical & Aerospace Engineering at the University of Texas at Arlington for providing support for the research work.

Table of Contents

List of Illustrations

List of Tables

Chapter 1

Introductions

1.1. Finite Element Method

Finite Element Method (FEM) is widely used in structural analysis. FEM makes it possible to analyze complex structure numerically by dividing the complex structure into small pieces and using elements to represent those small pieces. Therefore, the complex structure becomes a set of elements and can be computed simply.

With the development of FEM, researchers are improving the accuracy of elements. There are several ways to improve elements, like increase the order of elements, increase nodes of elements and increase Degrees of Freedom (DOFs) of elements and so on. The advantage of introducing rotational DOFs (or called drilling DOFs) are threefold. (1) Add more DOFs to the element without introducing more nodes in the element. (2) Relatively easier to implement than adding internal bubble and (3) Compatible with neighboring element.

1.2. Review of elements with rotational DOFs

In 1984, Allman [1], proposed a convenient method to introducing rotational DOFs into a triangular membrane element and get an accurate result. Bergan and Felippa in 1985 [2] proposed a similar element with a different approach. Then in 1986, Cook [3] showed that Allman's element can be derived by a transformation technique and can be easily extended to the quadrilateral element.

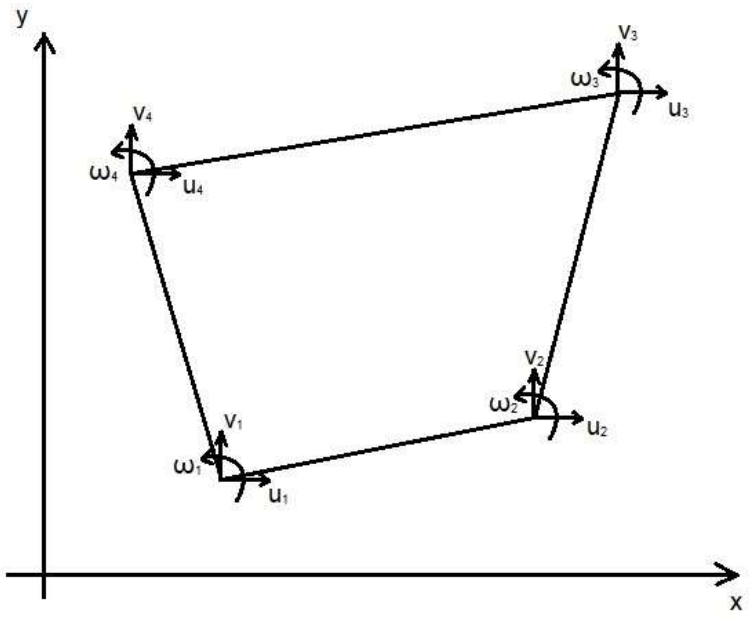

Figure 1-1 Element with rotational DOFs

After the rotational DOFs been successfully introduced into membrane element, many improvements and refining have been made. In 1988, Macneal and Harder [4] proposed a refined element which by adding auxiliary strain functions to Allman's element. In 1993, Long and Xu [5] presented new element using the approach of generalized conforming finite element.

Since most researchers proposed element and perform just statics problem test, how the rotational DOFs affects mass matrix and the application in dynamics analysis are still uncertain. Therefore, this work will investigate the effect of rotational DOFs in dynamics analysis and design optimization.

1.3. Scope of research

Since the objective is to investigate the influence of rotational DOFs in statics, dynamics, and optimization, the easy way is to start from the 2D element. To simplify the programming process, further, limit the range of element to isoperimetric quadrilateral

element. Specifically, three representative elements are implemented and applied to several test problems. The influence of rotational DOF would be observed in those test results.

1.4. Manuscript organization

In Chapter 2, the three elements formulation used in this work were introduced with the extension to the derivation of mass matrix for each element. In Chapter 3, several statics tests results are presented. The results are compared to the original result from the references to validate that these elements are correctly implemented in this work. Chapter 4 presents the results of dynamics test. Next, in Chapter 5 show the design optimization cases using the element with drilling DOF and compare to the standard element. Finally, in Chapter 6, make conclusions and proposed some possible future works.

Chapter 2

Elements with Rotational DOF

2.1. Introduction

This chapter introduces three elements used in the thesis then briefly describe other available elements. The three elements used in the thesis were selected based on the following requirements.

First, the chosen elements should only have four nodes, 12 DOFs, namely 3 DOFs per node. Any non-nodal DOFs should be eliminated during computing process. With this requirement, the total DOFs of any numerical test should be same. In addition, using these elements, the process of generating mesh will be much easier because there is no need to consider any mid-side nodes or internal nodes.

Second, the chosen elements should use isoperimetric coordinates in shape function. This requirement allows further simplified and uniformed computing process.

2.2. Element AQ

2.2.1. Introduction

Element AQ is short for Allman Quadrilateral. Namely, it is a quadrilateral element constructed by Allman's method. In 1984, Allman [1] proposed an approach to introducing rotational DOFs into a triangular element, then in 1986, Cook [3] derived Allman's triangular element by a different method called coordinate transformation approach and extended it to the quadrilateral element. Allman [6] also derived a quadrilateral element with rotational DOFs by his method in 1988.

2.2.2. *Shape function*

Note that each node has 3 DOFs $[u, v, \omega]$. The u, v DOFs are the normal in plane displacement in x, y direction respectively, and ω is the 'vertex rotation' [1] or 'nodal rotation' [3].

By Allman's method, first, choose the normal and tangential components of displacement u_n and u_t along element side 1-2 as Figure 2-1 shown and assume as:

$$\begin{aligned} u_n &= a_1 + a_2\, s + a_3\, s^2 \\ u_t &= a_4 + a_5 s \end{aligned} \qquad \text{2-1}$$

where s is measured from point 1 along the side and a_1 to a_5 are the coefficients.

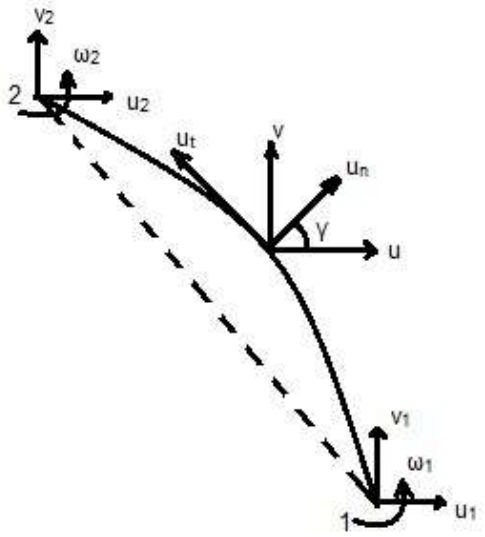

Figure 2-1 Edge displacement caused by ω_1 and ω_2

To determine the five unknown coefficients, there should have five equations. The first four equations are boundary conditions at edge ends, thus

$$\begin{aligned} u_{(n|s=0)} &= u_{n1}, u_{(n|s=l)} = u_{n2} \\ u_{(t|s=0)} &= u_{t1}, u_{(t|s=l)} = u_{t2} \end{aligned} \qquad \text{2-2}$$

where $u_{n1}, u_{t1}, \ldots$, etc. are calculate from the nodal displacement by the equation

$$\begin{Bmatrix} u_n \\ u_t \end{Bmatrix} = \begin{bmatrix} \cos\gamma & \sin\gamma \\ -\sin\gamma & \cos\gamma \end{bmatrix} \begin{Bmatrix} u \\ v \end{Bmatrix} \quad 2\text{-}3$$

where γ is the angle measure from x-direction to the normal direction of the edge.

The fifth equation comes from the edge displacement is

$$\frac{\partial u_n}{\partial s}_{s=l} - \frac{\partial u_n}{\partial s}_{s=0} = -\omega_2 + \omega_1 \quad 2\text{-}4$$

where ω_1 and ω_2 are rotational DOFs at the element node. Clearly, ω_1 and ω_2 are not the true rotation defined by the elastic theorem as $\omega = \frac{1}{2}\left(\frac{\partial v}{\partial x} - \frac{\partial u}{\partial y}\right)$

Now, the coefficient a_1 to a_5 can be solved as

$$\begin{aligned} a_1 &= u_{n1} \\ a_2 &= \frac{(u_{n2} - u_{n1})}{l} + \frac{(\omega_2 - \omega_1)}{2} \\ a_3 &= \frac{(\omega_1 - \omega_2)}{2l} \\ a_4 &= u_{t1} \\ a_5 &= \frac{(u_{t1} - u_{t2})}{l} \end{aligned} \quad 2\text{-}5$$

then submit equation 2-5 into equation 2-1 gives

$$\begin{aligned} u_n &= \left(1 - \frac{s}{l}\right) u_{n1} + \left(\frac{s}{l}\right) u_{n2} + \frac{1}{2} s \left(1 - \frac{s}{l}\right) (\omega_2 - \omega_1) \\ u_t &= \left(1 - \frac{s}{l}\right) u_{t1} + \left(\frac{s}{l}\right) u_{t2} \end{aligned} \quad 2\text{-}6$$

Finally, the displacement u and v can be computed by submit equation 2-6 into equation 2-3 and after simplification gives

$$\begin{Bmatrix} u \\ v \end{Bmatrix} = [N]\{q\}$$

where $\{q\} = (u_1, v_1, \omega_1, \dots, u_4, v_4, \omega_4)^T$ and

$$\begin{aligned} [N] &= \begin{bmatrix} N_1 & 0 & N_{u\omega 1} & N_2 & 0 & N_{u\omega 2} & N_3 & 0 & N_{u\omega 3} & N_4 & 0 & N_{u\omega 4} \\ 0 & N_1 & N_{v\omega} & 0 & N_2 & N_{v\omega 2} & 0 & N_3 & N_{v\omega 3} & 0 & N_4 & N_{v\omega} \end{bmatrix} \\ &= \begin{bmatrix} N_1 & 0 & (N_8\delta y_{14} - N_5\delta y_{21}) & N_2 & 0 & (N_5\delta y_{21} - N_6\delta y_{32}) \\ 0 & N_1 & (N_5\delta x_{21} - N_8\delta x_{14}) & 0 & N_2 & (N_6\delta x_{32} - N_5\delta x_{21}) \\ N_3 & 0 & (N_6\delta y_{32} - N_7\delta y_{43}) & N_4 & 0 & (N_7\delta y_{43} - N_8\delta y_{14}) \\ 0 & N_3 & (N_7\delta x_{43} - N_8\delta x_{12}) & 0 & N_4 & (N_8\delta x_{14} - N_7\delta x_{43}) \end{bmatrix} \end{aligned} \quad 2\text{-}7$$

in which

$$N_i = \frac{1}{4}(1+\xi_i\xi)(1+\eta_i\eta) \quad (i=1,2,3,4)$$

$$\begin{Bmatrix} N_5 \\ N_6 \\ N_7 \\ N_8 \end{Bmatrix} = \frac{1}{16}\begin{bmatrix} (1-\xi^2)(1-\eta) \\ (1+\xi)(1-\eta^2) \\ (1-\xi^2)(1+\eta) \\ (1-\xi)(1-\eta^2) \end{bmatrix}$$

$$\delta x_{ij} = x_i - x_j, \qquad \delta y_{ij} = y_i - y_j \quad (i,j = 1,2,3,4)$$

From equation 2-7, the terms N_1 to N_4 are the same as the standard quadrilateral element. The coordinates transformation between the Cartesian coordinate and the isoperimetric coordinates can use the same method as

$$\begin{Bmatrix} x \\ y \end{Bmatrix} = [N(s,t)]\{xy_i\} = \begin{bmatrix} N_1 & 0 & N_2 & 0 & N_3 & 0 & N_4 & 0 \\ 0 & N_1 & 0 & N_2 & 0 & N_3 & 0 & N_4 \end{bmatrix} \begin{Bmatrix} x_1 \\ y_1 \\ x_2 \\ y_2 \\ x_3 \\ y_3 \\ x_4 \\ y_4 \end{Bmatrix} \qquad 2\text{-}8$$

where the N_1 to N_4 is defined in previous equation and x_1, y_1 to x_4, y_4 is the nodal coordinates in Cartesian coordinate. By submitting the s and t in isoperimetric coordinates, can get the corresponding x and y in Cartesian coordinate.

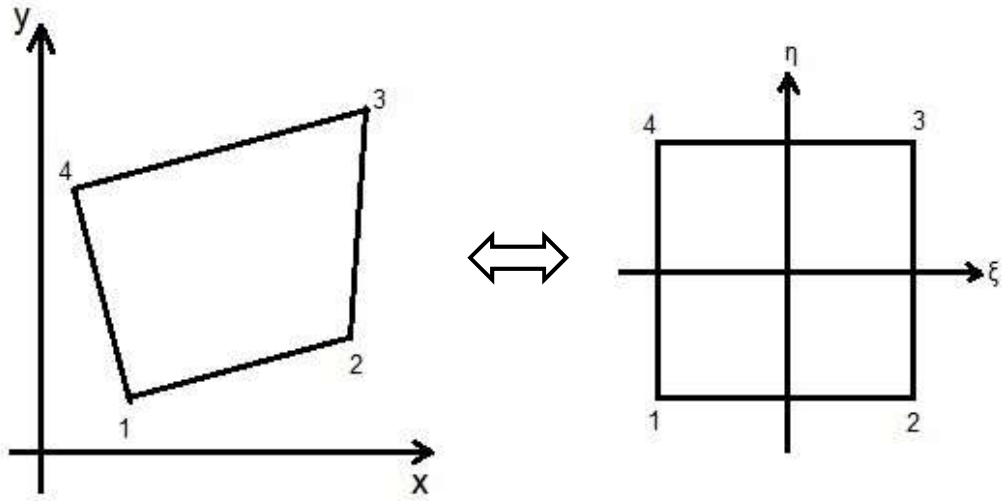

Figure 2-2 Coordinates transformation

The shape function plots are shown as following, color lines show contours of the shape function. From Figure 2-4 and Figure 2-5, the displacement caused by rotational DOFs is close to the displacement caused by the mid-side node. Cook [3] proved that the rotational DOFs formed by Allman's method is related to the tangential component of mid-side nod displacement and there is a transformation matrix used to obtain stiffness matrix of Allman's element from the element with mid-side nodes.

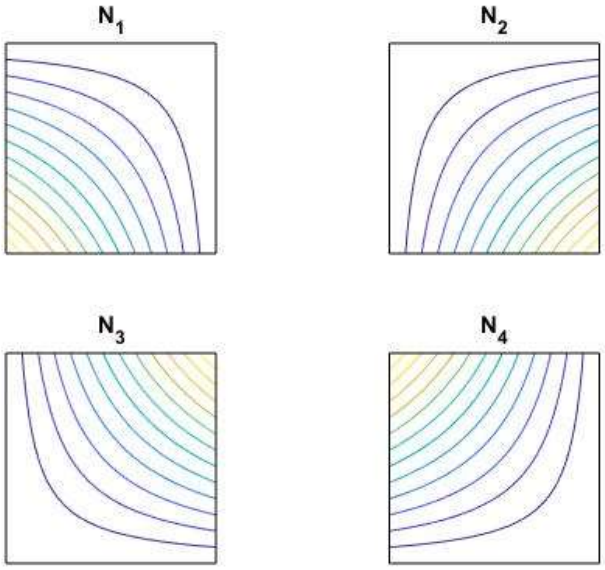

Figure 2-3 Shape function plot of element AQ

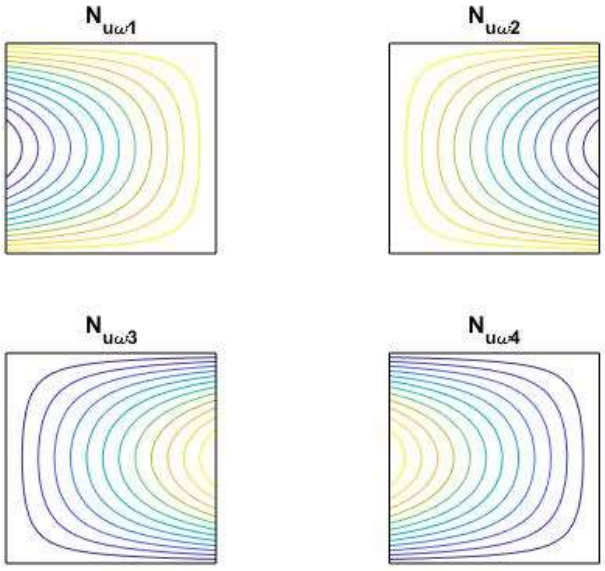

Figure 2-4 Shape function plot of element AQ

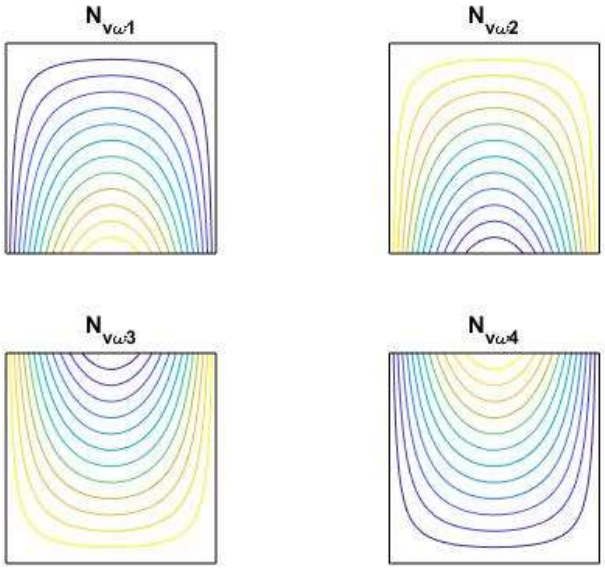

Figure 2-5 Shape function plot of element AQ

2.2.3. Stiffness matrix

Once having the shape function, then we can derive the stiffness matrix following the usual procedure. First, compute element strain as

$$\{\epsilon\} = \begin{Bmatrix} \epsilon_x \\ \epsilon_y \\ \gamma_{xy} \end{Bmatrix} = \begin{Bmatrix} \dfrac{\partial u}{\partial x} \\ \dfrac{\partial v}{\partial y} \\ \dfrac{\partial v}{\partial x} + \dfrac{\partial u}{\partial y} \end{Bmatrix} = \begin{bmatrix} \dfrac{\partial}{\partial x} & 0 \\ 0 & \dfrac{\partial}{\partial y} \\ \dfrac{\partial}{\partial y} & \dfrac{\partial}{\partial x} \end{bmatrix} \begin{Bmatrix} u \\ v \end{Bmatrix} = [\partial][N]\{q\} \qquad 2\text{-}9$$

where $[\partial]$ is the differential operation. By the chain rule of the derivative:

$$\begin{bmatrix} \dfrac{\partial N}{\partial \xi} \\ \dfrac{\partial N}{\partial \eta} \end{bmatrix} = \begin{bmatrix} \dfrac{\partial x}{\partial \xi} & \dfrac{\partial y}{\partial \xi} \\ \dfrac{\partial x}{\partial \eta} & \dfrac{\partial y}{\partial \eta} \end{bmatrix} \begin{bmatrix} \dfrac{\partial N}{\partial x} \\ \dfrac{\partial N}{\partial y} \end{bmatrix} = [J] \begin{bmatrix} \dfrac{\partial N}{\partial x} \\ \dfrac{\partial N}{\partial y} \end{bmatrix} \qquad 2\text{-}10$$

where $[J]$ is the Jacobian matrix and let

$$[\Gamma] = [J]^{-1} = \begin{bmatrix} \frac{\partial \xi}{\partial x} & \frac{\partial \eta}{\partial x} \\ \frac{\partial \xi}{\partial y} & \frac{\partial \eta}{\partial y} \end{bmatrix} \tag{2-11}$$

In addition,

$$[\partial][N] = \begin{bmatrix} \frac{\partial N(1,:)}{\partial x} \\ \frac{\partial N(2,:)}{\partial y} \\ \frac{\partial N(2,:)}{\partial x} + \frac{\partial N(1,:)}{\partial y} \end{bmatrix} = \begin{bmatrix} 1 & 0 & 0 & 0 \\ 0 & 0 & 0 & 1 \\ 0 & 1 & 1 & 0 \end{bmatrix} \begin{bmatrix} \frac{\partial N(1,:)}{\partial x} \\ \frac{\partial N(1,:)}{\partial y} \\ \frac{\partial N(2,:)}{\partial x} \\ \frac{\partial N(2,:)}{\partial y} \end{bmatrix} = [H_1] \begin{bmatrix} \frac{\partial N(1,:)}{\partial x} \\ \frac{\partial N(1,:)}{\partial y} \\ \frac{\partial N(2,:)}{\partial x} \\ \frac{\partial N(2,:)}{\partial y} \end{bmatrix} \tag{2-12}$$

where $N(1,:)$ is the first row of matrix N and $N(2,:)$ is the second row of matrix N. Thus,

$$\begin{bmatrix} \frac{\partial N(1,:)}{\partial x} \\ \frac{\partial N(1,:)}{\partial y} \\ \frac{\partial N(2,:)}{\partial x} \\ \frac{\partial N(2,:)}{\partial y} \end{bmatrix} = \begin{bmatrix} \frac{\partial N(1,:)}{\partial \xi}\frac{\partial \xi}{\partial x} + \frac{\partial N(1,:)}{\partial \eta}\frac{\partial \eta}{\partial x} \\ \frac{\partial N(1,:)}{\partial \xi}\frac{\partial \xi}{\partial y} + \frac{\partial N(1,:)}{\partial \eta}\frac{\partial \eta}{\partial y} \\ \frac{\partial N(2,:)}{\partial \xi}\frac{\partial \xi}{\partial x} + \frac{\partial N(2,:)}{\partial \eta}\frac{\partial \eta}{\partial x} \\ \frac{\partial N(2,:)}{\partial \xi}\frac{\partial \xi}{\partial y} + \frac{\partial N(2,:)}{\partial \eta}\frac{\partial \eta}{\partial y} \end{bmatrix} = \begin{bmatrix} \frac{\partial \xi}{\partial x} & \frac{\partial \eta}{\partial x} & 0 & 0 \\ \frac{\partial \xi}{\partial y} & \frac{\partial \eta}{\partial y} & 0 & 0 \\ 0 & 0 & \frac{\partial \xi}{\partial x} & \frac{\partial \eta}{\partial x} \\ 0 & 0 & \frac{\partial \xi}{\partial y} & \frac{\partial \eta}{\partial y} \end{bmatrix} \begin{bmatrix} \frac{\partial N(1,:)}{\partial \xi} \\ \frac{\partial N(1,:)}{\partial \eta} \\ \frac{\partial N(2,:)}{\partial \xi} \\ \frac{\partial N(2,:)}{\partial \eta} \end{bmatrix}$$

$$= \begin{bmatrix} \Gamma & 0 \\ 0 & \Gamma \end{bmatrix} \begin{bmatrix} \frac{\partial N(1,:)}{\partial \xi} \\ \frac{\partial N(1,:)}{\partial \eta} \\ \frac{\partial N(2,:)}{\partial \xi} \\ \frac{\partial N(2,:)}{\partial \eta} \end{bmatrix} = [H_2][H_3] \tag{2-13}$$

Then, the element strain matrix can be written as

$$[B] = [\partial][N] = [H_1][H_2][H_3] \tag{2-14}$$

The strain energy U can be written as

$$U = \frac{t}{2}\iint_A \{\varepsilon\}^T[D]\{\varepsilon\}dA = \frac{t}{2}\iint_A \{q\}^T[B]^T[D][B]\{q\}dA$$

$$= \frac{1}{2}\{q\}^T\left(t\iint_A [B]^T[D][B]dA\right)\{q\} \tag{2-15}$$

then, get stiffness matrix as

$$[K] = \iint_A t[B]^T[D][B]dA = t\int_{-1}^{1}\int_{-1}^{1}[B]^T[D][B]|J|d\xi d\eta \qquad 2\text{-}16$$

where t is the thickness of the element, ξ and η are the isoperimetric coordinates, $|J|$ is the determinant of the Jacobian matrix, $[D]$ is the elasticity matrix of the isotropic material for plane stress.

2.2.4. Mass matrix

The mass matrix can be derived by the usual procedure.

$$[M] = \int_A t\,\rho[N]^T[N]\,dA = t\rho\int_{-1}^{1}\int_{-1}^{1}[N]^T[N]|J|d\xi d\eta \qquad 2\text{-}17$$

where ρ is the density of the element.

2.2.5. Load vector

The load vector can be derived by the usual procedure.

$$\{F\} = \int_{l_{ij}}[N]^T\{P\}ds \qquad 2\text{-}18$$

where $\{P\} = [p_x \quad p_y]^T$, and p_x, p_y are the external forces on the boundary l_{ij} of the element, along x and y directions, respectively.

2.3. Element GQ12M

2.3.1. Introduction

Element GQ12M is proposed by Long and Xu [7] at 1993. This element is constructed with the generalized conforming approach, and a bubble displacement is introduced to improve the performance.

2.3.2. Shape function

According to Long and Xu, the element displacement can be divided into three parts

$$\{u\} = \{u^0\} + \{u_\theta\} + \{\hat{u}\} \qquad 2\text{-}19$$

where $\{u^0\}$ is the conventional bilinear compatible displacement, $\{u_\theta\}$ is the displacement due to vertex rotation and $\{\hat{u}\}$ is the bubble displacement to refine the displacement field. The $\{u^0\}$ given as

$$\{u^0\} = \begin{Bmatrix} u^0 \\ v^0 \end{Bmatrix} = [N^0] \begin{Bmatrix} u_i \\ v_i \end{Bmatrix} = \sum_{i=1}^{4} \begin{bmatrix} N_i^0 & 0 \\ 0 & N_i^0 \end{bmatrix} \begin{Bmatrix} u_i \\ v_i \end{Bmatrix} \tag{2-20}$$

in which

$$N_i^0 = \frac{1}{4}(1 + \xi_i \xi)(1 + \eta_i \eta) \tag{2-21}$$

where ξ_i and η_i are the isoperimetric coordinates at each node respectively.

The additional displacement $\{u_\theta\}$ are assumed as

$$\begin{aligned} u_\theta &= (1-\xi^2)(\alpha_1 + \alpha_2 \eta) + (1-\eta^2)(\alpha_3 + \alpha_4 \xi) \\ v_\theta &= (1-\eta^2)(\beta_1 + \beta_2 \xi) + (1-\xi^2)(\beta_3 + \beta_4 \eta) \end{aligned} \tag{2-22}$$

where α_i and β_i are the arbitrary parameters. The boundary displacement along each side due to the node rotation can be written as cubic functions as

$$\begin{aligned} u_{\theta ij} &= \frac{1}{8}(y_i - y_j)(1-\xi^2)\left[\theta_i(1-\xi) - \theta_j(1+\xi)\right] \\ v_{\theta ij} &= \frac{1}{8}(x_i - x_j)(1-\xi^2)\left[\theta_i(1-\xi) - \theta_j(1+\xi)\right] \end{aligned} \quad (i,j) = (1,2),(3,4)$$

$$\begin{aligned} u_{\theta ij} &= \frac{1}{8}(y_i - y_j)(1-\eta^2)\left[\theta_i(1-\eta) - \theta_j(1+\eta)\right] \\ v_{\theta ij} &= \frac{1}{8}(x_i - x_j)(1-\eta^2)\left[\theta_i(1-\eta) - \theta_j(1+\eta)\right] \end{aligned} \quad (i,j) = (1,3),(2,4)$$

where x_i and y_i are the Cartesian coordinates of element nodes. For each side, the generalized compatibility conditions are given by

$$\iint_{l_{ij}} u_\theta ds = \int_{l_{ij}} u_{\theta ij} ds\,, \qquad \iint_{l_{ij}} v_\theta ds = \int_{l_{ij}} v_{\theta ij} ds$$

Then the parameters α_i and β_i can be expressed in terms of θ_i. Finally, $\{u_\theta\}$ can be expressed as

$$\{u_\theta\} = \sum_{i=1}^{4} \begin{Bmatrix} N_{u\theta i} \\ N_{v\theta i} \end{Bmatrix} \theta_i$$

where

$$N_{u\theta i} = \frac{1}{8}[\xi_i(1-\xi^2)(b_1+b_3\eta_i)(1+\eta_i\eta)+\eta_i(1-\eta^2)(b_2+b_3\xi_i)(1+\xi_i\xi)]$$
$$N_{v\theta i} = \frac{1}{8}[\xi_i(1-\xi^2)(a_1+a_3\eta_i)(1+\eta_i\eta)+\eta_i(1-\eta^2)(a_2+a_3\xi_i)(1+\xi_i\xi)]$$

in which,

$$a_1 = \frac{1}{4}\sum_{i=1}^{4}\xi_i x_i \quad a_2 = \frac{1}{4}\sum_{i=1}^{4}\eta_i x_i \quad a_3 = \frac{1}{4}\sum_{i=1}^{4}\xi_i\eta_i x_i$$
$$b_1 = \frac{1}{4}\sum_{i=1}^{4}\xi_i y_i \quad b_2 = \frac{1}{4}\sum_{i=1}^{4}\eta_i y_i \quad b_3 = \frac{1}{4}\sum_{i=1}^{4}\xi_i\eta_i y_i$$

The bubble displacement is defined as

$$\{\hat{u}\} = [\hat{N}]\{\rho\} = \begin{bmatrix} \hat{N} & 0 \\ 0 & \hat{N} \end{bmatrix} \begin{Bmatrix} \rho_1 \\ \rho_2 \end{Bmatrix} \qquad 2\text{-}23$$

in which $\hat{N} = (1-\xi^2)(1-\eta^2)$ and ρ_1 and ρ_2 are arbitrary independent parameters and will be eliminated in the following process.

Therefore, the displacement is given as

$$\{u\} = [N]\{q\} + [\hat{N}]\{\rho\} = \sum_{i=1}^{4} \begin{bmatrix} N_i^0 & 0 & N_{u\theta i} \\ 0 & N_i^0 & N_{v\theta i} \end{bmatrix} \begin{Bmatrix} u_i \\ v_i \\ \theta_i \end{Bmatrix} + \begin{bmatrix} \hat{N} & 0 \\ 0 & \hat{N} \end{bmatrix} \begin{Bmatrix} \rho_1 \\ \rho_2 \end{Bmatrix} \qquad 2\text{-}24$$

It is easy to prove that the shape function [N] in element GQ12M is same as the shape function [N] in element AQ, just substitute all the parameter, and then the equation becomes identical. The components of shape function of element AQ and GQ12M for u_i and v_i terms are the same. For the components of shape function for ω_i, the component relating u and ω_1 of element AQ is

$$N_{u\omega} = N_8\delta y_{14} - N_5\delta y_{21} = \frac{1}{16}(1-\xi)(1-\eta^2)(y_1-y_4) - \frac{1}{16}(1-\xi^2)(1-\eta)(y_2-y_1)$$

Moreover, the corresponding term in shape function of element GQ12M is

$$N_{u\theta 1} = \frac{1}{8}[\xi_1(1-\xi^2)(b_1+b_3\eta_1)(1+\eta_1\eta)+\eta_1(1-\eta^2)(b_2+b_3\xi_1)(1+\xi_1\xi)]$$

$$= \frac{1}{8}[-(1-\xi^2)(b_1-b_3)(1-\eta)-(1-\eta^2)(b_2-b_3)(1-\xi)]$$

$$= \frac{1}{8}\left[-(1-\xi^2)\left(\frac{1}{4}(-y_1+y_2+y_3-y_4)-\frac{1}{4}(y_1-y_2+y_3-y_4)\right)(1-\eta)\right.$$

$$\left.-(1-\eta^2)\left(\frac{1}{4}(-y_1-y_2+y_3+y_4)-\frac{1}{4}(y_1-y_2+y_3-y_4)\right)(1-\xi)\right]$$

$$= \frac{1}{8}\left[-(1-\xi^2)\left(\frac{1}{2}(-y_1+y_2)\right)(1-\eta)-(1-\eta^2)\left(\frac{1}{2}(-y_1+y_4)\right)(1-\xi)\right]$$

$$= \frac{1}{16}(1-\xi)(1-\eta^2)(y_1-y_4)-\frac{1}{16}(1-\xi^2)(1-\eta)(y_2-y_1)$$

Thus, $N_{u\omega 1} = N_{u\theta 1}$, and other corresponding term in shape function of element AQ and element GQ12M can be proved to be identical following the same procedure.

The shape function plots of [N] are the same as element AQ. The shape function of bubble displacement plot is shown as following, color lines show contours of the shape function.

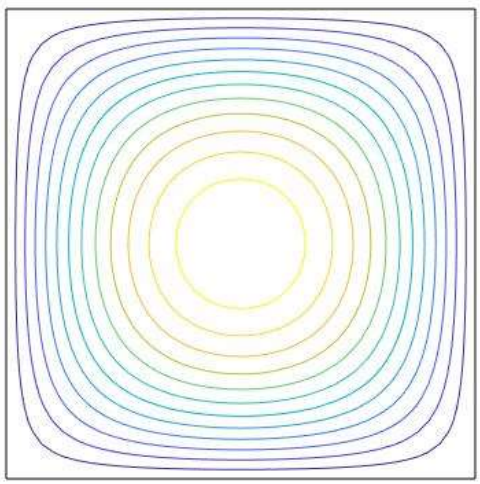

Figure 2-6 Shape function plot of bubble displacement of element GQ12M

2.3.3. *Stiffness matrix*

The strain can be written as

$$\{\varepsilon\} = [B]\begin{Bmatrix} u_i \\ v_i \\ \theta_i \end{Bmatrix} + \left[\hat{B}\right]\begin{Bmatrix} \rho_1 \\ \rho_2 \end{Bmatrix} \tag{2-25}$$

where $\{\varepsilon\}$ is the vector of the strain, $[B]$ is the strain matrix and $\left[\hat{B}\right]$ is the strain matrix of bubble displacement which can be computed as the same procedure as element AQ.

The strain energy U can be written as

$$U = \frac{t}{2}\iint_A \{\varepsilon\}^T[D]\{\varepsilon\}dA = \frac{1}{2}\{q\}^T\left[K_{qq}\right]\{q\} + \{\rho\}^T\left[K_{\rho q}\right]\{q\} + \frac{1}{2}\{\rho\}^T\left[K_{\rho\rho}\right]\{\rho\} \tag{2-26}$$

where $\{q\} = (u_1, v_1, \omega_1, \dots, u_4, v_4, \omega_4)^T$ is nodal displacement and $\{\rho\} = (\rho_1, \rho_2)^T$ is bubble displacement,

$$\left[K_{qq}\right] = t\int_{-1}^{1}\int_{-1}^{1}[B]^T[D][B]|J|d\xi d\eta$$
$$\left[K_{\rho q}\right] = t\int_{-1}^{1}\int_{-1}^{1}\left[\hat{B}\right]^T[D][B]|J|d\xi d\eta$$
$$\left[K_{\rho\rho}\right] = t\int_{-1}^{1}\int_{-1}^{1}\left[\hat{B}\right]^T[D]\left[\hat{B}\right]|J|d\xi d\eta$$

From the condition that strain energy is independent of bubble displacement parameters, namely, $\frac{\partial U}{\partial\{\rho\}} = \{0\}$,

$$\frac{\partial U}{\partial\{\rho\}} = \left[K_{\rho q}\right]\{q\} + \left[K_{\rho\rho}\right]\{\rho\} = \{0\} \tag{2-27}$$

Then, the parameters can be obtained in terms of $\{q\}$

$$\{\rho\} = -\left[K_{\rho\rho}\right]^{-1}\left[K_{\rho q}\right]\{q\} \tag{2-28}$$

Therefore, by substitute equation 2-28 into equation 2-24, yields

$$\{u\} = [N]\{q\} - \left[\widehat{N}\right]\left[K_{\rho\rho}\right]^{-1}\left[K_{\rho q}\right]\{q\} = [N_e]\{q\} \tag{2-29}$$

where

$$[N_e] = [N] - \left[\widehat{N}\right]\left[K_{\rho\rho}\right]^{-1}\left[K_{\rho q}\right]$$

By substitute equation 2-27 and 2-28 into equation 2-26, the strain energy yields

$$U = \frac{1}{2}\{q\}^T[K_{qq}]\{q\} - \frac{1}{2}\{q\}^T[K_{\rho q}]^T[K_{\rho\rho}]^{-1}[K_{\rho\rho}][K_{\rho\rho}]^{-1}[K_{\rho q}]\{q\}$$
$$= \frac{1}{2}\{q\}^T\left([K_{qq}] - [K_{\rho q}]^T[K_{\rho\rho}]^{-1}[K_{\rho q}]\right)\{q\} \quad 2\text{-}30$$

Thus, the stiffness matrix can be written as

$$[K] = [K_{qq}] - [K_{\rho q}]^T[K_{\rho\rho}]^{-1}[K_{\rho q}] \quad 2\text{-}31$$

2.3.4. Mass matrix

The mass matrix can also be derived by the usual procedure.

$$[M] = \int_A t\,\rho[N_e]^T[N_e]\,dA = t\rho\int_{-1}^{1}\int_{-1}^{1}[N_e]^T[N_e]|J|d\xi d\eta \quad 2\text{-}32$$

where ρ is the density of the element.

2.3.5. Load vector

The load vector can be derived by the usual procedure.

$$\{F\} = \int_{l_{ij}}[N_e]^T\{P\}ds \quad 2\text{-}33$$

where $\{P\} = [p_x \quad p_y]^T$, and p_x, p_y are the external forces on the boundary l_{ij} of the element, along x and y directions, respectively.

2.4. Element QA4

2.4.1. Introduction

In 1993, Chen and Li [8] proposed an element developed by the refined direct stiffness method. This element includes Allman's conforming displacement function and non-conforming function with four internal displacements. This element is the element QA4 in this thesis.

2.4.2. Shape function

The displacement of the QA4 element is divided into two parts

$$\{u\} = \{u_e\} + \{u_\lambda\} = [N]\{q\} + [N_\lambda]\{\lambda\} \quad 2\text{-}34$$

where $[N]$ is the shape function of Allman's quadrilateral element (equation 2-7) and $[N_\lambda]$ and λ are non-conforming function and internal displacement. The purpose of adding such internal displacement is to refine the element displacement field.

The non-conforming shape function is chosen to be

$$[N_\lambda] = \begin{bmatrix} \xi^2(1+\eta^2) & \eta^2(1+\xi^2) & 0 & 0 \\ 0 & 0 & \xi^2(1+\eta^2) & \eta^2(1+\xi^2) \end{bmatrix} \quad 2\text{-}35$$

The plot of shape function of internal displacement is shown as following, the color lines show contours of the shape function.

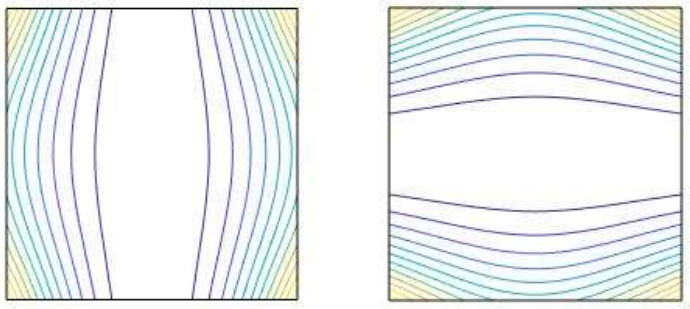

Figure 2-7 Shape function plot of internal displacement of element QA4

2.4.3. Stiffness matrix

The strain can be written as

$$\{\varepsilon\} = [B]\begin{Bmatrix} u_i \\ v_i \\ \theta_i \end{Bmatrix} + [B_\lambda]\begin{Bmatrix} \lambda_1 \\ \lambda_2 \\ \lambda_3 \\ \lambda_4 \end{Bmatrix} \quad 2\text{-}36$$

where $\{\varepsilon\}$ is the vector of the strain, λ_i is the internal displacement, $[B]$ is the strain matrix and $[B_\lambda]$ is the strain matrix of internal non-conforming displacement.

Usually, elements with non-conforming displacement cannot pass the patch test. Therefore, Chen and Li [8] proposed to construct a new $[B_\lambda^*]$ based on $[B_\lambda]$ by refined direct stiffness method to enable the element to pass the patch test. Let

$$[B_{\lambda 0}^*] = \frac{1}{\Delta}\int_v [B_\lambda] dv = \frac{8}{3\Delta}\begin{bmatrix} b & -b & 0 & 0 \\ 0 & 0 & -a & a \\ -a & a & b & -b \end{bmatrix} \quad 2\text{-}37$$

where $\Delta = \int_v dv$ is the volume of the element, $a = \frac{1}{4}(x_1 - x_2 + x_3 - x_4)$ and $b = \frac{1}{4}(y_1 - y_2 + y_3 - y_4)$. Then the new strain matrix can be defined as

$$[B_\lambda^*] = [B_\lambda] - [B_{\lambda 0}^*] \quad 2\text{-}38$$

Therefore, the strain become

$$\{\varepsilon\} = [B]\begin{Bmatrix} u_i \\ v_i \\ \theta_i \end{Bmatrix} + [B_\lambda^*]\begin{Bmatrix} \lambda_1 \\ \lambda_2 \\ \lambda_3 \\ \lambda_4 \end{Bmatrix} \quad 2\text{-}39$$

The strain energy U can be written as

$$U = \frac{t}{2}\iint_A \{\varepsilon\}^T[D]\{\varepsilon\} dA = \frac{1}{2}\{q\}^T\left[K_{qq}\right]\{q\} + \{\lambda\}^T\left[K_{\lambda q}\right]\{q\} + \frac{1}{2}\{\lambda\}^T[K_{\lambda\lambda}]\{\lambda\} \quad 2\text{-}40$$

where

$$\left[K_{qq}\right] = t\int_{-1}^{1}\int_{-1}^{1}[B]^T[D][B]|J|d\xi d\eta$$
$$\left[K_{\lambda q}\right] = t\int_{-1}^{1}\int_{-1}^{1}[B_\lambda^*]^T[D][B]|J|d\xi d\eta$$
$$[K_{\lambda\lambda}] = t\int_{-1}^{1}\int_{-1}^{1}[B_\lambda^*]^T[D][B_\lambda^*]|J|d\xi d\eta$$

Then, follow the same procedure as element GQ12M, from $\frac{\partial U}{\partial\{\lambda\}} = \{0\}$, the internal displacements can be obtained as

$$\{\lambda\} = -[K_{\lambda\lambda}]^{-1}\left[K_{\lambda q}\right]\{q\} \quad 2\text{-}41$$

Therefore, the displacement function becomes

$$\{u\} = [N]\{q\} - [N_\lambda][K_{\lambda\lambda}]^{-1}\left[K_{\lambda q}\right]\{q\} = [N_e]\{q\} \tag{2-42}$$

where the shape function is

$$[N_e] = [N] - [N_\lambda][K_{\lambda\lambda}]^{-1}\left[K_{\lambda q}\right] \tag{2-43}$$

moreover, the stiffness matrix can be written as

$$[K] = \left[K_{qq}\right] - \left[K_{\lambda q}\right]^T[K_{\lambda\lambda}]^{-1}\left[K_{\lambda q}\right] \tag{2-44}$$

2.4.4. Mass matrix

The mass matrix can also be derived by the usual procedure.

$$[M] = \int_A t\,\rho[N_e]^T[N_e]\,dA = t\rho\int_{-1}^{1}\int_{-1}^{1}[N_e]^T[N_e]|J|d\xi d\eta \tag{2-45}$$

2.4.5. Load vector

The load vector can be derived by the usual procedure.

$$\{F\} = \int_{l_{ij}}[N_e]^T\{P\}ds \tag{2-46}$$

where $\{P\} = [p_x \quad p_y]^T$, and p_x, p_y are the external forces on the boundary l_{ij} of the element, along x and y directions, respectively.

2.5. Other elements with rotational DOF

Beside the elements mention above, there are several other elements with rotational DOFs. They include hybrid elements, elements with area coordinates, elements formed by variational formulation and so on.

Some researchers proposed elements with rotational DOFs formed by different schemes. In 1989, Stander and Wilson [9] proposed a quadrilateral element with rotational DOFs formed by degeneration of the 9-node Lagrange element. In 1992, Sze, Chen, and Cheung [10] proposed an element with rotational DOFs by refining the stress modes of Allman's quadrilateral element.

Several researchers proposed hybrid elements. In 1987, Cook [11] proposed a plane hybrid triangular element using assumed-stress hybrid approach. In 1989, Yunus, Saigal, and Cook [12] proposed a set of three new hybrid elements with rotational DOFs. In 1992, Aminpour [13] [14] proposed assumed-stress hybrid shell elements with rotational DOFs. In 2006, Choi, Choo and Lee [15] presented triangular and quadrilateral hybrid Trefftz element with rotational DOFs. In 2015, Chen and el. [16] proposed a generalized conforming membrane element with rotational DOFs using area coordinates.

Some mathematics papers discussed forming element with rotational DOFs by using variational formulation. In 1992, Simo, Fox, and Hughes [17] discussed the variational formulations for the element with the independent rotational field. In 1993, Cazzani and Atluri [18] proposed a family of 4-node elements with rotational DOFs which derived from a mixed variational formula.

Chapter 3

Statics Analysis and Validation

3.1. Introduction

In this chapter, six selected numerical test problems of statics analysis will be solved to show that the elements with rotational DOFs have better performance. In addition, the comparison between the results in this work and results from references will also validate the implementation of those elements in this work.

The elements used in this chapter are listed below:

Q4: traditional 4-node 8-DOF quadrilateral element

AQ: 4-node 12-DOF quadrilateral element proposed by Allman [6]

GQ12M: 4-node 12-DOF quadrilateral element proposed by Long and Xu [7]

QA4: 4-node 12-DOF quadrilateral element proposed by Chen and Li [8]

The numerical integrations are carried out with Gauss quadrature using 4x4 Gauss points. Thus, use 4 points along ξ-direction, 4 points along η-direction. The reason to using 4x4 Gauss points is the rotational components of shape function contain $\xi^2\eta$ and $\xi\eta^2$ term, so the integral for stiffness matrix and mass matrix will contain higher order term. Therefore, full integration demands 4x4 Gauss points to get enough accuracy.

The computing environment is Matlab running on 64bit Windows 10 computer, and the detailed function description and data structure will be presented in Appendix A.

3.2. Patch test

The purpose of patch test is that, if an element passes the patch test, the computed results with this element under mesh refinement would converge for any other problem. The mesh of the patch test should contain a subdivided area so that the number

of elements will change along the section. There are many different patch test meshes used by researchers. In this work, the mesh of patch test is shown in Figure 3-1.

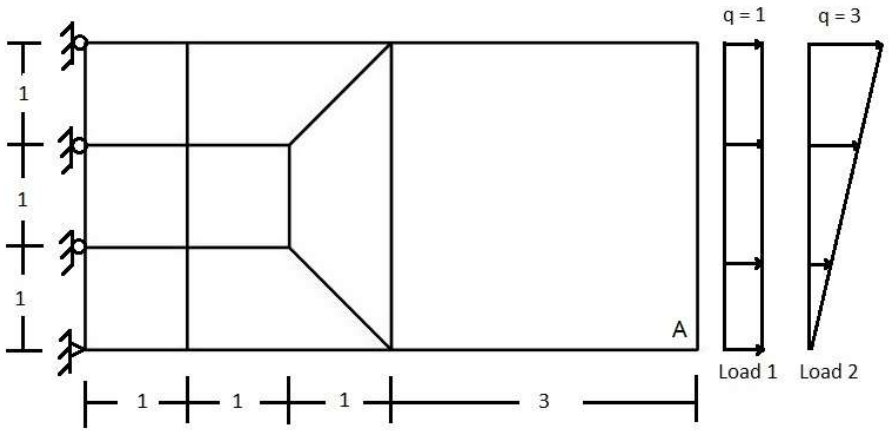

Figure 3-1 Patch test

This patch test was used by some researchers [7] to perform both patch test and bending test. As Figure 3-1 shows, a beam under two loading condition at the right end. Load 1 represents a patch test, and load 2 represents bending behavior. The length and height are shown in figure, and the thickness is 1.

Table 3-1 Patch test

Element	Load 1		Load 2
	U_A	Patch Test	V_A
Q4	6.00	Pass	-14.89
AQ	6.00	Pass	-17.31
GQ12M	6.00	Pass	-17.59
QA4	6.00	Pass	-17.72
Exact	6.00	-	-18.00

The test results are presented in Table 3-1. It demonstrates that all the elements can produce correct result with load 1, so they all pass the patch test. However, with load 2, the result of Q4 element is far from the exact result while all the elements with rotational DOFs have better results.

3.3. Macneal's thin cantilever beam

This test was proposed by Macneal [19] to test the element performance when the element aspect ratio is increased, and element shape changed. As Figure 3-2 shown, a thin cantilever beam was fixed at left end and under a unit load at the right end. The length is 6, the width is 0.2, and the thickness is 0.1. Three different meshes are shown in Figure 3-2.

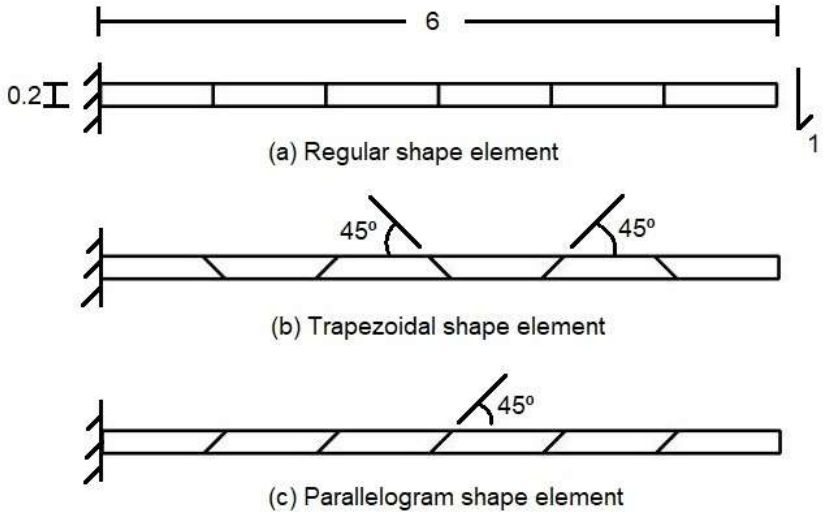

E = 1.0x10^7, $\nu = 0.30$

Figure 3-2 Macneal's thin cantilever beam

The results are presented in Table 3-2. The data of 'QA4 ref.' row is collected from Chen and Lee [8], and the results are same as the results produced in this work. As expected, the Q4 element has poor performance in this test, and the result is worse with

element distortion. In contrast, the element with rotational DOFs perform good and can get very close results, and the results did not change much with element distortion. Therefore, the element with rotational DOFs is insensitive to high aspect ratio and element distortion.

Table 3-2 Macneal's thin cantilever beam

Element	Regular	Trapezoidal	Parallelogram
Q4	-0.0101	-0.0029	-0.0037
AQ	-0.0977	-0.0825	-0.0909
GQ12M	-0.1056	-0.0956	-0.0994
QA4	-0.1073	-0.0989	-0.1038
QA4 ref. [8]	-0.1073	-0.0989	-0.1038
Exact [19]	-0.1081	-0.1081	-0.1081

3.4. Tip-loaded cantilever beam

This test problem is used by Allman [6] and Long [7] to test their elements with rotational DOFs. As the Figure 3-3 shown, a beam is fixed at left end and under 40000 load at the right end. The length and height are showing in the figure, and the thickness of the beam is 1. It was modeled by four quadrilateral elements. This is a simple test to check the element performance.

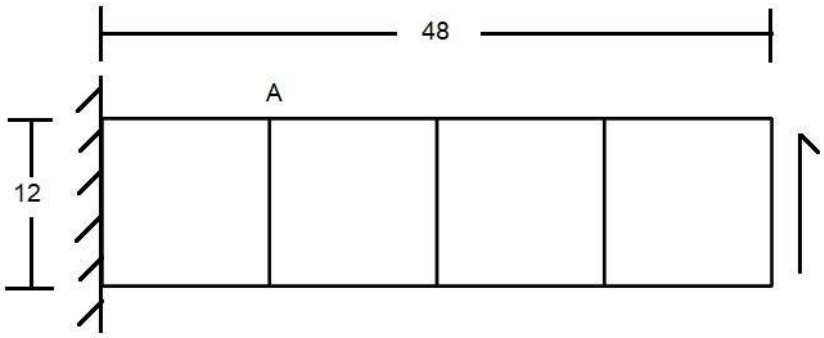

E = 3x10^7, $\nu = 0.25$

Figure 3-3 Tip-loaded cantilever beam.

The numerical results computed using different elements are given in Table 3-3, and the results from references also included, and it shows that the results of elements with rotational DOFs performed better than the traditional element.

Table 3-3 Tip-loaded cantilever beam

Element	V_{tip}	σ_x at A
Q4	0.2424	-43.64
AQ	0.3283	-60.0
AQ ref. [6]	0.3283	-
GQ12M	0.3446	-63.09
GQ12M ref. [7]	0.3446	-60.65
QA4	0.3493	-60.0
Comparison [3]	0.3573	-60.0

3.5. Tip-loaded cantilever beam with irregular mesh

As Figure 3-4 shown, the tip-loaded cantilever beam with irregular mesh has same geometry size but different mesh with the previous test. This test was aimed to test the element performance with mesh distortion. The numerical results are given in Table 3-4, and the results from the references are also included.

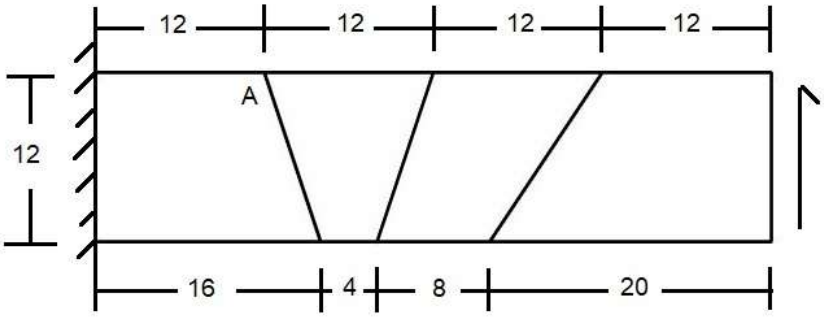

E = 3x10^7, $\nu = 0.25$

Figure 3-4 Tip-loaded cantilever beam with irregular mesh.

Table 3-4 Tip-loaded cantilever beam with irregular mesh

Element	Q4	AQ	AQ ref. [6]	GQ12M	QA4	Comparison [3]
V_{tip}	0.2096	0.3330	0.3379	0.3412	0.3462	0.3573
σ_x at A	-37.96	-60.99	-	-62.69	-58.05	-60

As the result shown in Table 3-4, the Q4 element has poor result, and it is sensitive to mesh distortion since the result in this problem is worse than the result in Table 3-3. By comparing the results in Table 3-3 and Table 3-4, it shows that the elements with rotational DOFs are insensitive to mesh distortion.

3.6. Cook's Problem

The test case shown in Figure 3-5 was first proposed by Cook [20]. The geometry dimension is shown in the figure, and the thickness is 1.

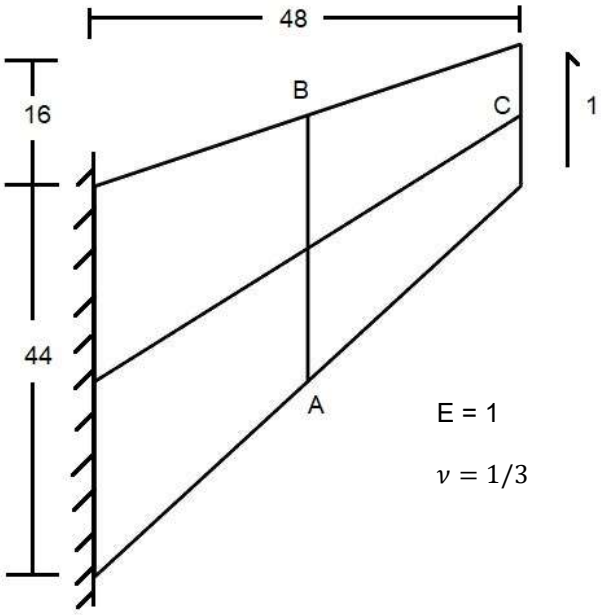

Figure 3-5 Cook's problem

The results are given in Table 3-5, and the results from references are also included. There are six meshes in the table, researchers are usually computed first three meshes, but other three meshes are added to test element convergence. The convergence results are shown in Figure 3-6. The stress results presented in Table 3-6.

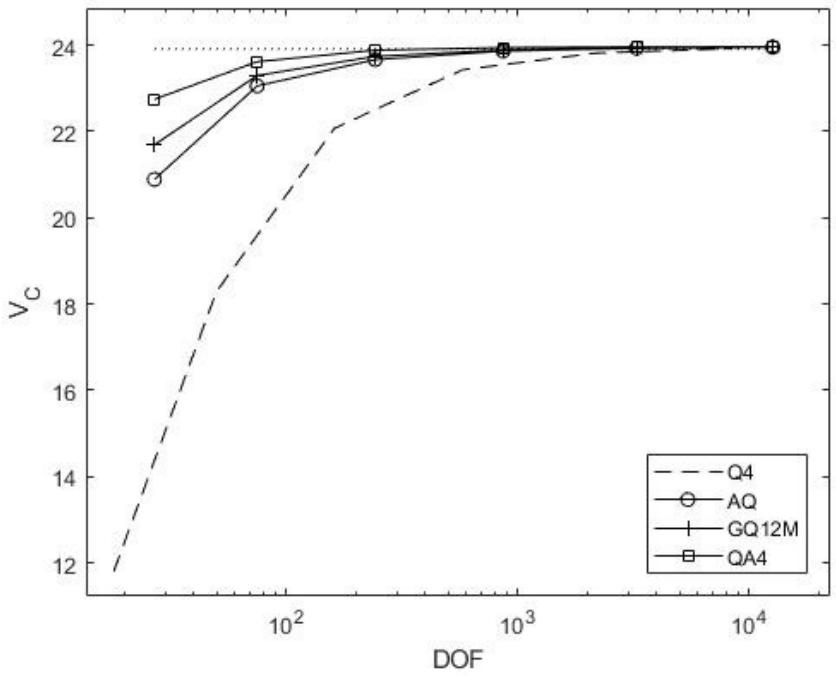

Figure 3-6 Convergence of Cook's problem

Table 3-5 Deflection at C of Cook's problem

Element	2x2	4x4	8x8	16x16	32x32	64x64
Q4	11.80	18.29	22.08	23.43	23.81	23.92
AQ	20.89	23.06	23.67	23.86	23.93	23.95
AQ ref. [6]	20.89	23.06	23.67	-	-	-
GQ12M	21.69	23.30	23.74	23.89	23.94	23.96
GQ12M ref. [7]	21.69	23.30	23.74	-	-	-
QA4	22.75	23.61	23.88	23.95	23.96	23.96
QA4 ref. [8]	23.29	23.78	-	-	-	-
Reference [20]	23.90					

As Figure 3-6 shown, the results of all elements will converge to the reference result, but the elements with rotational DOFs converge much faster than the standard element. In Table 3-5, the results show that the elements with rotational perform well in the coarse mesh. In Table 3-6, the results also show that the elements with rotational DOFs get more accurate stress results than Q4 element with coarse mesh.

Table 3-6 Stress analysis of Cook's problem

Mesh / Element	σ_1 at A			σ_2 at B		
	2x2	4x4	8x8	2x2	4x4	8x8
Q4	0.1278	0.1905	0.2251	-0.0908	-0.1508	-0.1866
AQ	0.1796	0.2219	0.2320	-0.1786	-0.1965	-0.2010
GQ12M	0.1887	0.2204	0.2289	-0.1783	-0.1937	-0.2025
QA4	0.2080	0.2438	0.2458	-0.2267	-0.2107	-0.2146
Reference [20]	0.2360			-0.2010		

3.7. Plate with hole

In this example, a plate with a center-located circular hole under plane stress is considered. The purpose of this example is to determine the performance of element with stress concentration. Due to symmetry, a quarter of the plate is modeled in Figure 3-7. The length and height of the quarter model are shown in Figure 3-7.

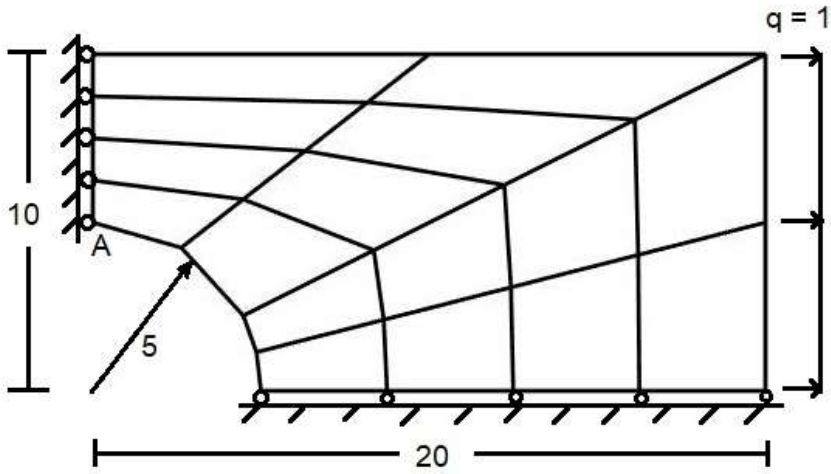

E = 50, $\nu = 0.3$

Figure 3-7 Plate with hole

The thickness of the plate is 0.1. The radius of the circular hole is 5. The plate is under tension along the x-direction. The results are given in Table 3-1, and the reference results are computed by Q4 element with fine mesh shown below.

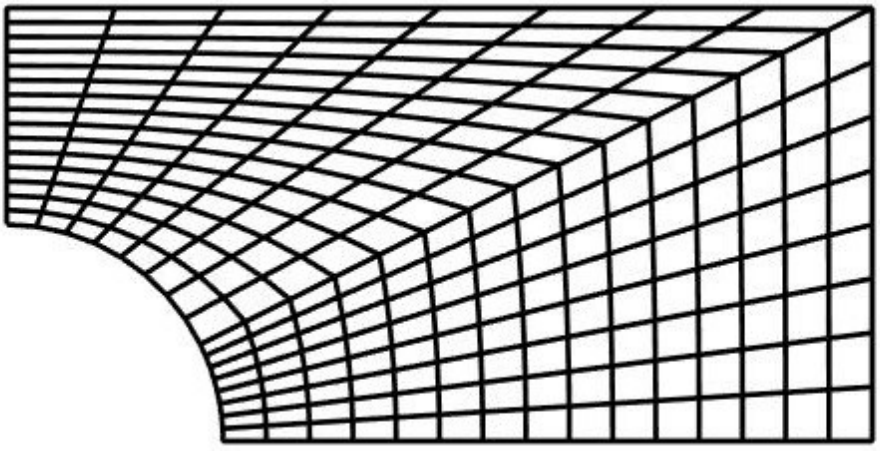

Figure 3-8 Fine mesh of plate with hole

Table 3-7 Plate with hole

Element	Q4	AQ	GQ12M	QA4	Reference
V_A	-1.50	-1.63	-1.56	-1.62	-2.08
σ_x at A	36.72	35.37	33.76	35.55	43.05

From Table 3-7, the results did not show significant differences between elements with and without rotational DOFs. All the elements did not get accurate results in this kind of stress concentration.

3.8. Element performance and validation

From the test results in this chapter, the performance of elements with rotational DOFs is better than the element without rotational DOFs, especially in coarse mesh and distorted mesh. In addition, the elements with rotational DOFs also performed well with high element aspect ratio.

By comparing between results that computed in this work and the results collected from references, it shows that the implementation of elements in this work can be considered as correct within an acceptable error. Those errors may be caused by different numbers of Gauss quadrature points or different computing environments.

Chapter 4

Dynamics Analysis

4.1. Introduction

Most researchers only performed FEM statics analysis when proposing an element and it is enough to in most cases. However, since the introduced rotational DOF is not the real elastic rotation in mechanics, the components in mass matrix caused by rotational term may lead to some uncertainty in dynamics analysis. In 2010, Karaköse and Askes [21] presented both statics and dynamics analysis of element with rotational DOFs and showed accuracy improvement in dynamics by using elements with rotational DOFs.

In this chapter, elements with rotational DOFs will be used in dynamics analysis. For each test problem, three types of results are computed, i.e., natural frequency (eigenvalue problem), time domain response at the specific point and frequency response.

4.2. Cantilever beam with tip load

As Figure 4-1 shown, a cantilever beam is fixed at left end and under loading at right end. The length and height are shown in the figure, and thickness of the beam is 1. It was under a step load of 4×10^5 which started from t = 0s. A proportional damping with coefficient $\alpha_K = 0.001$ was introduced. Thus, the damping matrix C is given by $C = \alpha_K K$.

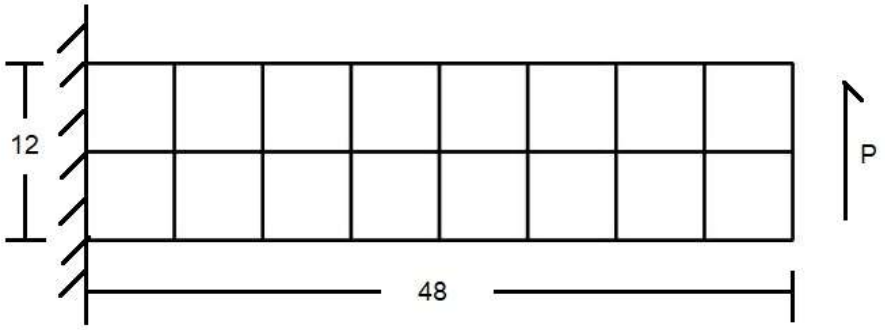

E = 7x10^7, $\nu = 0.3$, $\rho = 2700$, P = 4x10^5

Figure 4-1 Cantilever beam with tip load

4.2.1. Eigenvalue problem for cantilever beam

The results of natural frequency for cantilever beam are shown in Table 4-1, and the reference result is computed by a 32x8 mesh with Q4 element. From the results in Table 4-1, the QA4 element has the worst result, while the results of other elements are close to reference.

Table 4-1 Natural frequency of Cantilever beam

Element	First five natural frequencies				
Q4	0.8674	4.5319	5.3027	10.7876	16.0686
AQ	0.8303	4.2775	5.3019	9.9640	16.0532
GQ12M	0.8214	4.2243	5.2974	9.8467	15.9894
QA4	0.7980	3.8249	5.2675	7.9334	10.8197
Reference	0.8187	4.1690	5.2849	9.6092	15.5776

4.2.2. Time domain response for cantilever beam

Figure 4-2 shows the time domain response at the tip. Results by different elements are presented by different colors, and the 'comparison' result is computed by

Q4 element with 32x8 mesh are shown as dashed line. The results show that AQ element and GQ12M element are very close to ‘comparison’ result, and the Q4 element and QA4 element produced poor results.

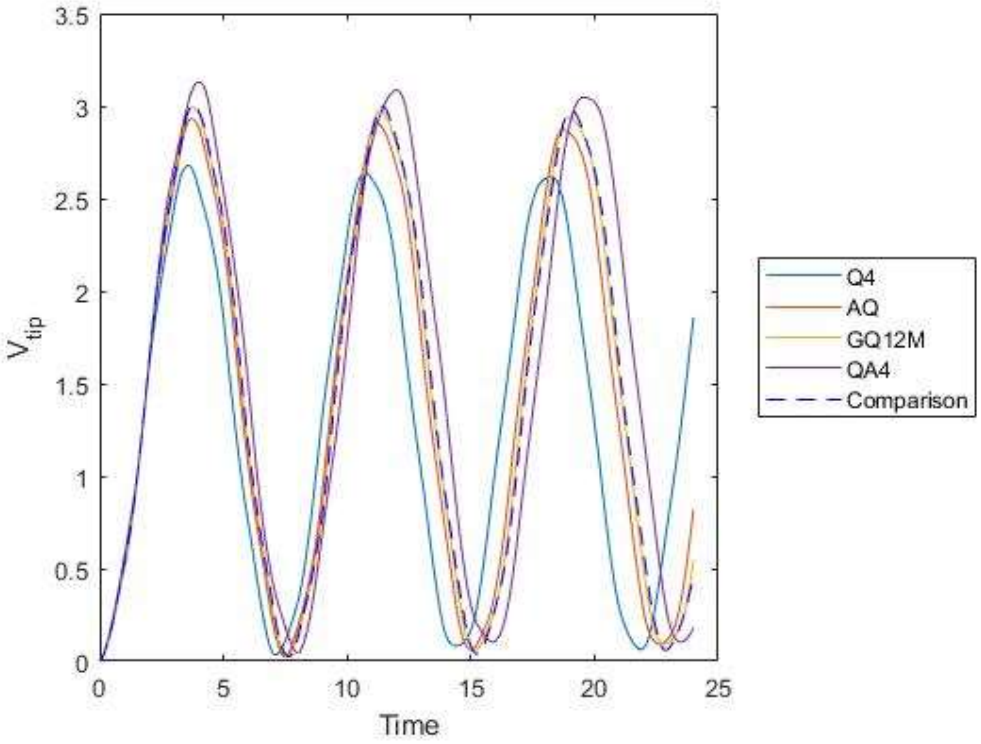

Figure 4-2 Response at tip for cantilever beam

4.2.3. Frequency response for cantilever beam

The frequency response of the cantilever beam is shown in Figure 4-3. The result shows that the peaks agree well in the short term but will deviate in the long term. The Q4 element and the QA4 element produced poor results while the results of AQ element and GQ12M element are close to ‘comparison’ result.

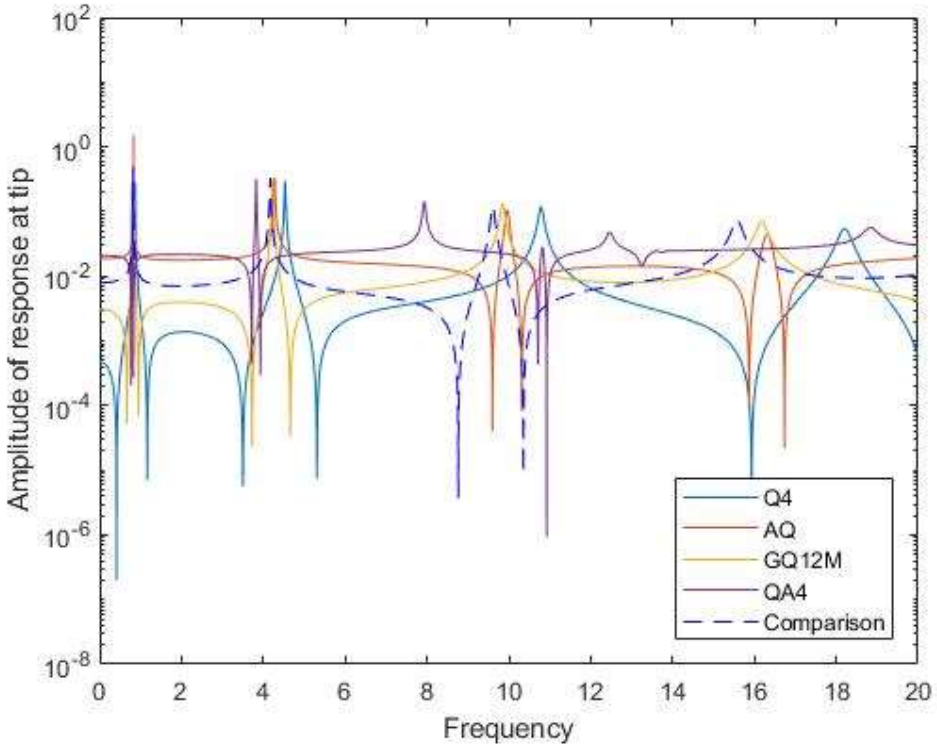

Figure 4-3 Frequency response for cantilever beam

4.3. Cantilever beam with narrowed tip under tip load

As Figure 4-4 shown, a cantilever beam with varied cross-section is fixed at left end and under loading at right end. The length and width are shown in the figure, and its thickness is 1. It was under a step load of $2/3 \times 10^5$ which started from t = 0s. A proportional damping with coefficient $\alpha_K = 0.001$ was introduced.

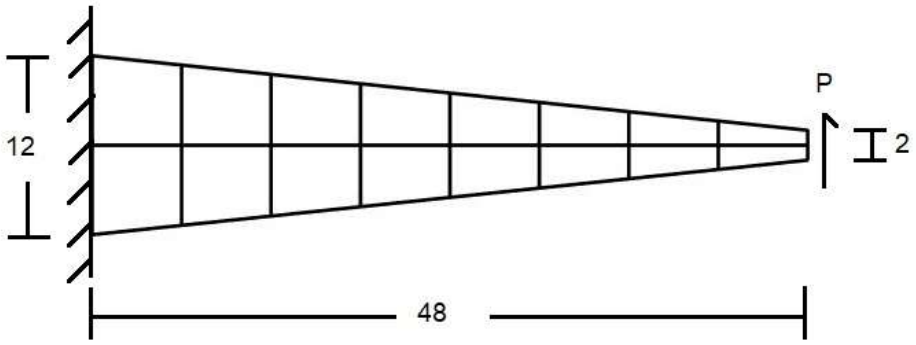

E = 7x10^7, $\nu = 0.3$, $\rho = 2700$, P = 2/3x10^5

Figure 4-4 Cantilever beam with narrowed tip under tip load

4.3.1. Eigenvalue problem for cantilever beam with narrowed tip

The results of natural frequency for cantilever beam with narrowed tip were given in Table 4-2. The results show elements with rotational DOFs are more accurate in general, but element QA4 produced poor results compare to other elements with rotational DOFs. Reference result was computed by 16x4 mesh with Q4 element

Table 4-2 Natural frequency of Cantilever beam with narrowed tip

Element	First five natural frequencies				
Q4	1.1382	4.0575	7.0720	9.0529	15.8627
AQ	1.0477	3.4798	7.0601	7.4389	12.6583
GQ12M	1.0382	3.4364	7.0595	7.3334	12.5049
QA4	1.0319	3.2561	6.8331	6.8629	10.9823
Reference	1.0419	3.4401	7.0481	7.2270	11.9945

4.3.2. Time domain response for cantilever beam with narrowed tip

Figure 4-5 shows the time domain response at the tip due to load, and the comparison result is computed by 16x4 mesh. Results by different elements are

presented by different colors. The results show that traditional Q4 element will get a worse result with course nonrectangular mesh. In addition, the results computed by element AQ and element GQ12M are close to the comparison results. However, the results produced by element QA4 show some different vibration pattern compare to all other results.

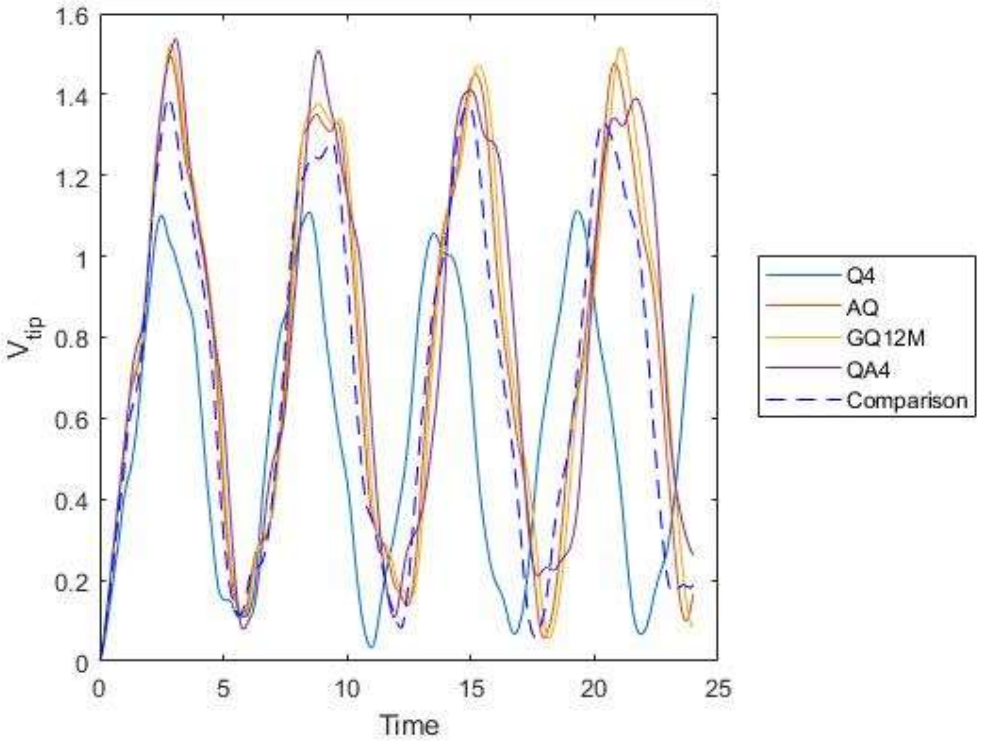

Figure 4-5 Response at tip for cantilever beam with narrowed tip

4.3.3. Frequency response for cantilever beam with narrowed tip

The frequency response was shown in Figure 4-6. Element AQ and element GQ12M produced similar results and close to comparison results. Element Q4 produced poor results, and element QA4 produced worst results.

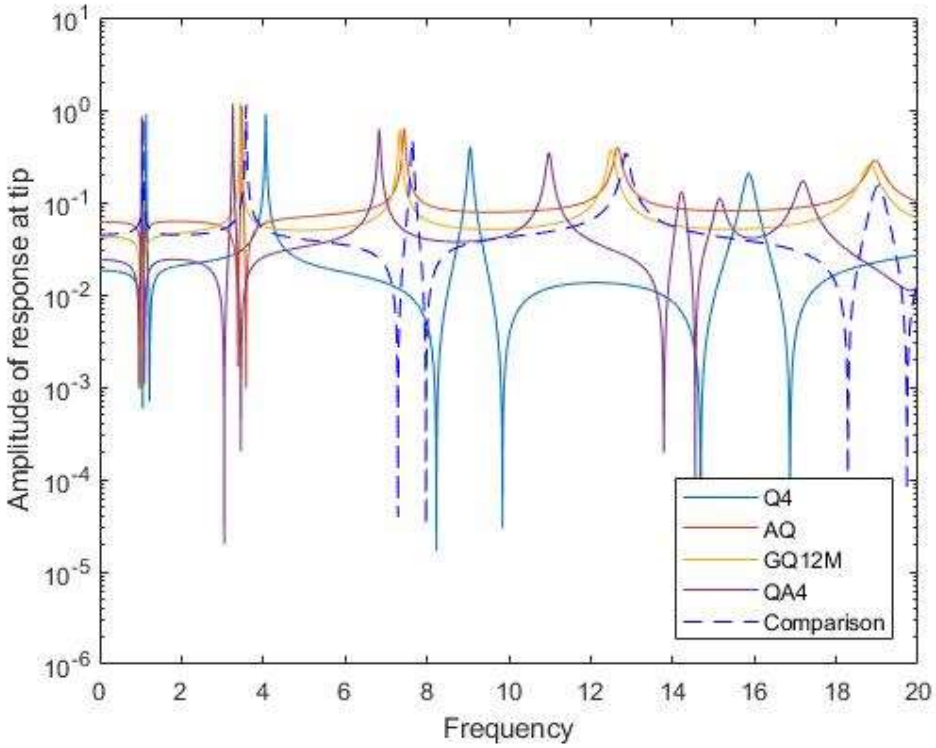

Figure 4-6 Frequency response for cantilever beam with narrowed tip

4.4. L-plate under tip load

As Figure 4-7 shown, an L-shape plate under tip load. The dimensions are marked on the figure, and the thickness of the plate is 1. The plate is fixed at the top and under a step load at right end started from t = 0s. This plate is modeled by 18 elements, and each element has same size.

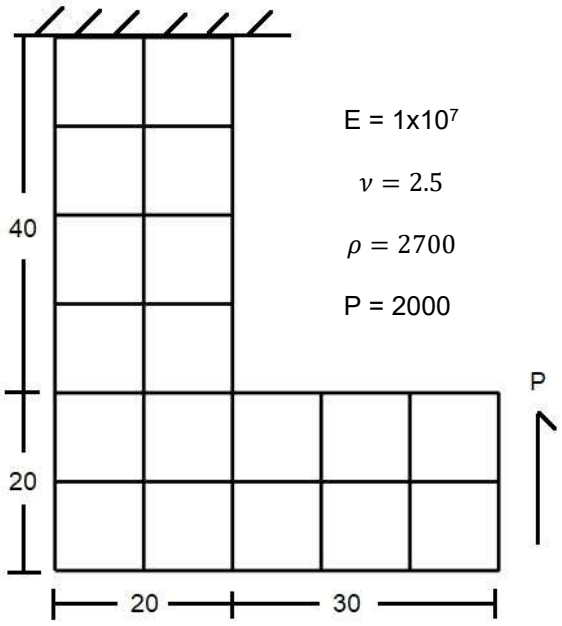

Figure 4-7 L-plate under tip load

4.4.1. Eigenvalue problem for L-plate

The results of natural frequency for L-plate are given in Table 4-3. As expected, the results of element AQ and element GQ12M are close to each other and lower than the results of element Q4. In addition, the result of element QA4 is different from other elements.

Table 4-3 Natural frequency of L-plate

Element	First five eigenvalues				
Q4	0.2008	0.6362	1.4808	2.1373	3.4250
AQ	0.1916	0.6099	1.4654	1.9929	3.2064
GQ12M	0.1900	0.6024	1.4619	1.9728	3.1893
QA4	0.1826	0.5524	1.4113	1.6486	2.3791

4.4.2. Time domain response for L-plate

As the Figure 4-8 shown, the AQ and GQ12M elements have the similar plot and have the same vibration pattern with element Q4, and the result of element QA4 is different from other elements.

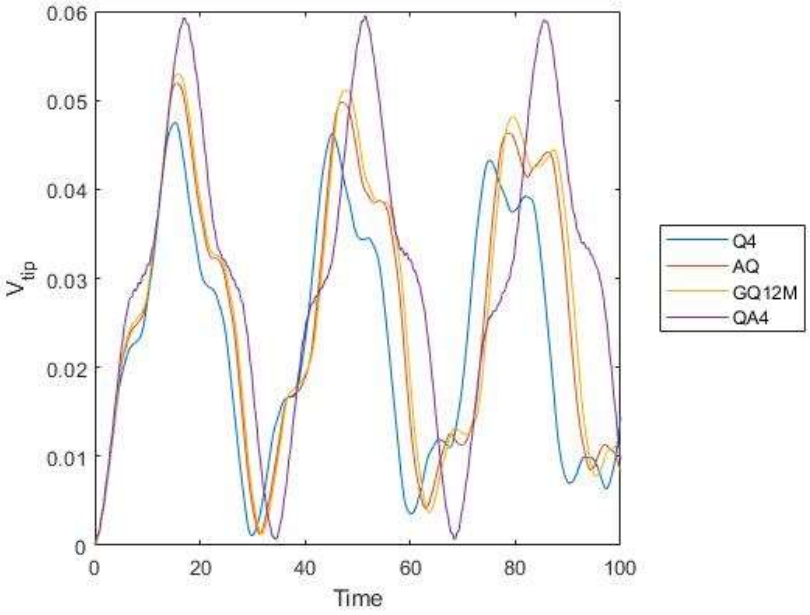

Figure 4-8 Response at tip for L-plate

4.4.3. Frequency response for L-plate

As Figure 4-9 shown, performed like previous test problem, Element AQ and element GQ12M produced similar results. Element Q4 produced poor results, and the results of element QA4 are far from other elements.

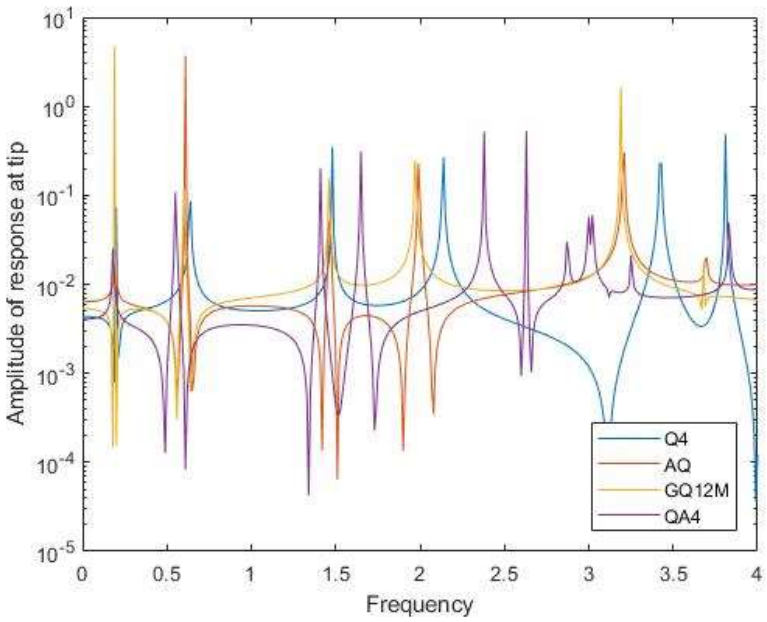

Figure 4-9 Frequency response for L-plate

4.5. Chapter conclusion

According to the results in this chapter, the elements with rotational DOFs will improve the performance in FEM dynamics analysis. However, the element with modified strain matrix, namely, QA4 element has poor results compared to other elements with rotational DOFs. It may because the strain field was refined but the shape function remains unchanged, so the stiffness matrix and the mass matrix may become mismatch.

Chapter 5

Optimal Design Using Elements with Rotational DOFs

5.1. Introduction

Optimal Design usually is to minimize the objective function like volume subjected to some constraints. Namely, to find the stiffest structure with minimum material. In this chapter, elements with drilling DOF will be applied to design optimization.

5.2. Sizing problem

5.2.1. Cantilever beam with varying tip

As Figure 5-1 shown, a cantilever beam was modeled by 4x2 mesh. The length and width of the beam are shown in the figure, and the thickness of the beam is 0.5. The initial width of right end is 30.

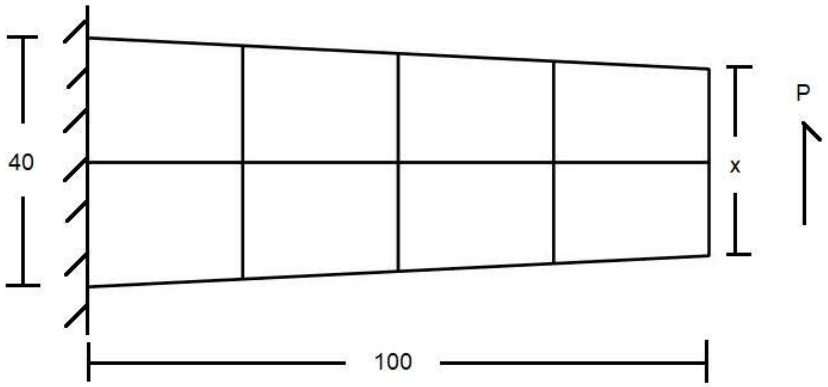

E = 7x10^7, $\nu = 0.3$

Figure 5-1 Cantilever beam varying tip

The objective of this problem is to find the optimal height of right end to minimize the volume of the beam under the constraint that all displacements due to tip load should be smaller than 1. The results are shown in Table 5-1 and Figure 5-2.

Table 5-1 Optimal tip

Element	Iteration	Width of tip	Volume
Q4	8	19.8909	1497.2722
AQ	7	27.0533	1676.3328
GQ12M	6	27.9221	1698.0536
QA4	7	31.5701	1789.2529

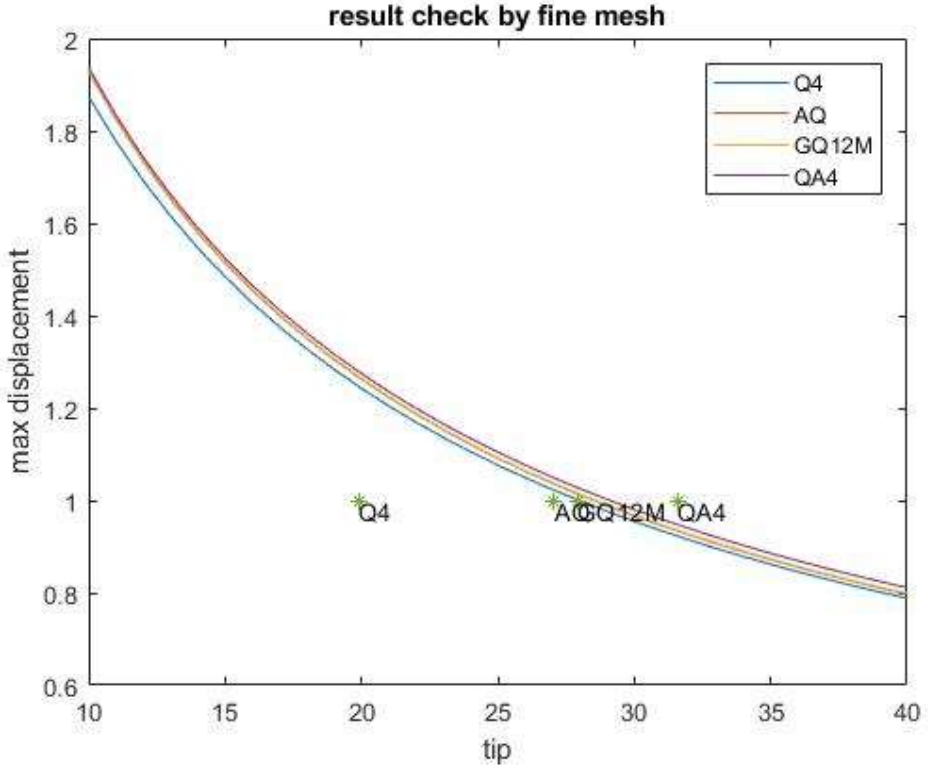

Figure 5-2 Optimal tip for statics constraint

As the results shown in Figure 5-2, those lines are computed by all element with a fine 16x8 mesh to illustrate how the max-displacement varies with the tip size and those points are the optimization results compute with a coarse 4x2 mesh. Comparing the results in Table 5-1 and Figure 5-2, it shows that the elements with rotational DOFs can get accurate results with coarse mesh in design optimization.

5.2.2. Cantilever beam with varying both tip and thickness

As Figure 5-3 shown, it is the same model with the previous problem, but both width of tip and thickness are the design variables. The bound for the width of tip is 10 to 40 and the bound for thickness is from 0.01 to 1. The objective of this problem is to find the optimal width of tip and thickness to minimize the volume of the beam under the constraint that all displacements due to tip load should be smaller than 1. The results are shown in Table 5-2 and Figure 5-4

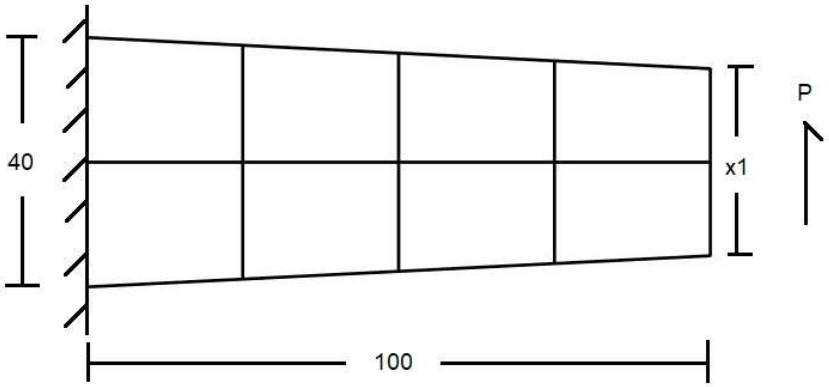

E = 7x10^7, $\nu = 0.3$

Figure 5-3 Cantilever beam varying both tip and thickness

Table 5-2 Optimal tip and thickness

Element	Iteration	Width of tip	Thickness	Volume
Q4	8	40	0.3325	1330.0236
AQ	6	40	0.3801	1520.3877
GQ12M	6	40	0.3892	1556.9046
QA4	6	40	0.4300	1719.9756

Figure 5-4 shows the displacement contour compute by element Q4 with a fine 16x8 mesh to illustrate how the variation of max-displacement with the width of tip and thickness, The design optimization results computed with a coarse mesh are marked on the figure. By comparing the results in Table 5-2 and Figure 5-4, it shows that the elements with rotational DOFs can get accurate results with coarse mesh in design optimization.

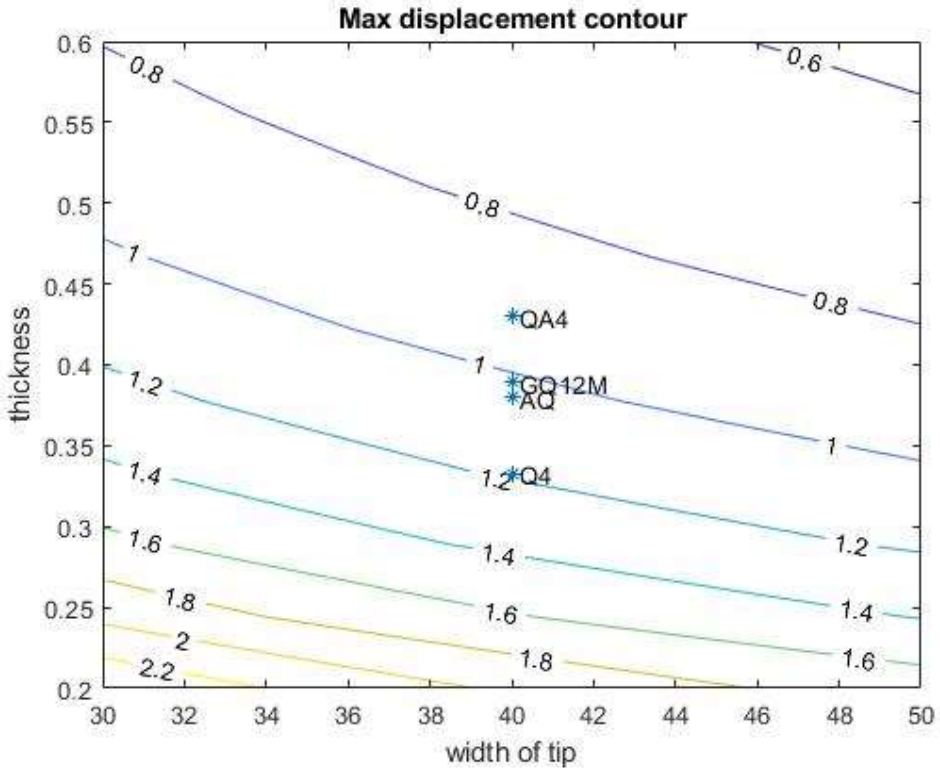

Figure 5-4 Contour of the tip and thickness

5.3. Topology optimization

The objective of a typical topology optimization problem is to minimize the compliance:

$$c(x) = \{u\}^T[K]\{u\} = \sum_{e=1}^{N} (x_e)^p \{u_e\}^T [K_e]\{u_e\}$$

where x is design variable, $\{u\}$ is global displacement, $[K]$ is global stiffness matrix, the terms with subscript e indicating it is represented for element term.

Subject to the constraints that

$$\begin{cases} \dfrac{V(x)}{V_0} = f \\ [K]\{u\} = \{F\} \\ 0 < x \leq 1 \end{cases}$$

where $V(x)$ and V_0 are the material volume and design volume, f is the volume fraction and $\{F\}$ is the global force vector.

In this section, design variable $\{x\}$ is relative densities of all elements, and optimization problem is solved using Optimality Criteria method and without any filter. The computing procedure and the coding of Optimality Criteria in this work is referenced from Sigmund [22]. In 2017, Balogh and Lógó [23] suggested that implementation of elements with rotational DOFs may prevent checkerboard phenomenon in topology optimization. The results of topology optimization by elements with rotational DOFs will be presented in the following sub-section.

5.3.1. Plate under corner load

As Figure 5-5 shown, the plate is fixed at left and under a vertical load at right bottom corner. The length and width of the beam are shown in the figure, and thickness is 1. The objective is to find the stiffest structure with given material (40% of total volume) under certain boundary conditions.

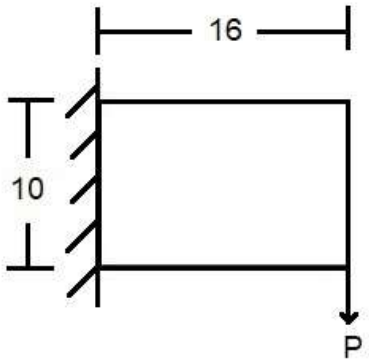

E = 1x10^7, $\nu = 0.3$, P = 2x10^4, 160x100 mesh

Figure 5-5 Cantilever beam under tip load

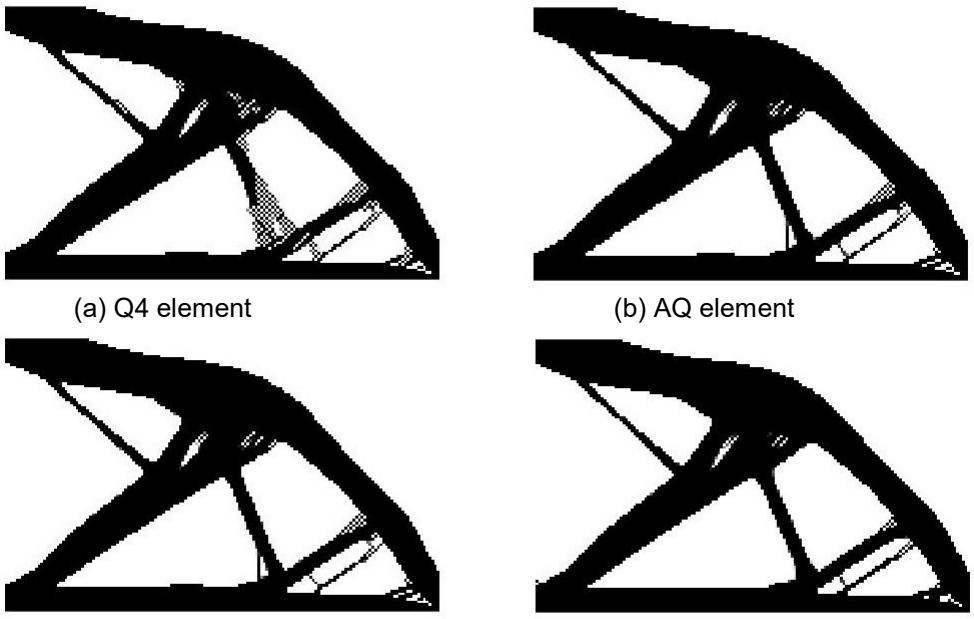

(a) Q4 element (b) AQ element

(c) GQ12M element (d) QA4 element

Figure 5-6 Topology optimization results for plate

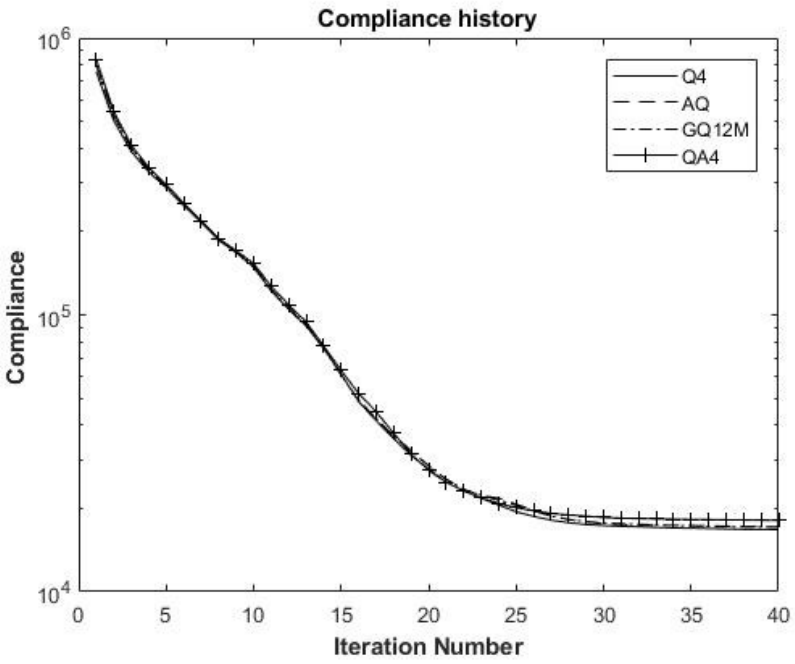

Figure 5-7 Compliance history

As Figure 5-6 and Figure 5-7 shown, the optimal results are converged to the similar result, and the optimal structure is similar. However, the result of Q4 element has serious checkerboard phenomenon.

5.3.2. L-shape plate under tip load

As Figure 5-8 shown, the L-shape plate under distribute loading on the right end, and the dimensions are marked on the figure. The mesh size is 0.5, and entirely 7200 elements are used in the mesh. The objective is to find the stiffest structure with given material (40% of total volume) under certain boundary conditions.

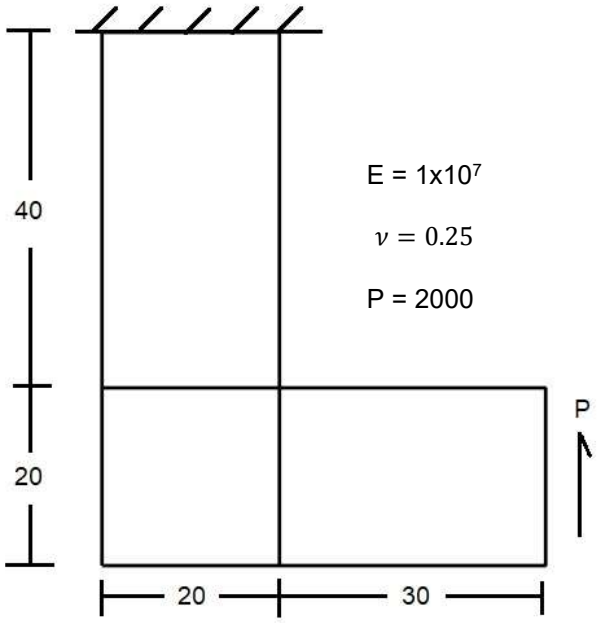

Figure 5-8 L-shape plate under tip load

The optimal results are shown in Figure 5-9 and Figure 5-10. As the figure shown, as the last test, the optimal results are converged to the similar result, and the optimal structure is similar, and the result of Q4 element have serious checkerboard phenomenon like the last test.

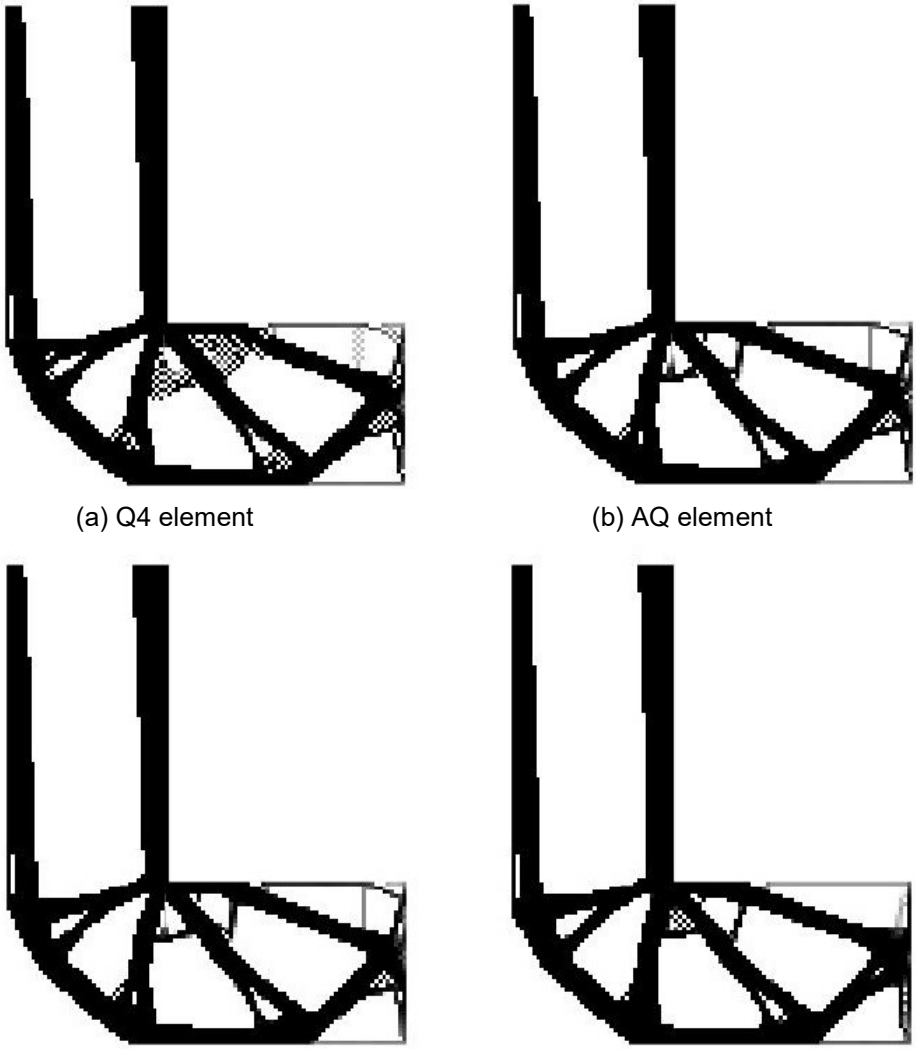

(a) Q4 element (b) AQ element

(c) GQ12M element (d) QA4 element

Figure 5-9 Topology optimization result for L-plate

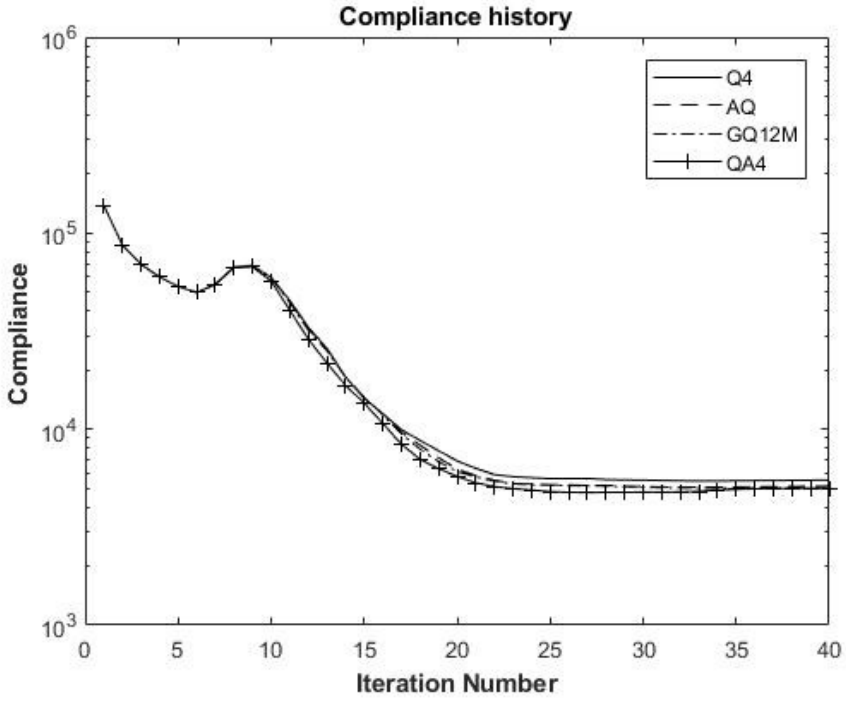

Figure 5-10 Compliance history

5.4. Chapter Conclusion

From the results of sizing problem in this chapter, it shows that the elements with rotational DOFs will improve the result accuracy in the coarse mesh. Therefore, elements with rotational DOFs can be used to generate a good initial design by performing optimal design with a coarse mesh. The design can further be refined with a fine mesh. It may decrease time cost in optimization.

For the results of topology optimization, implementation of elements with rotational DOFs can prevent checkerboard phenomenon in topology optimization even without a filter.

Chapter 6

Conclusion and Recommendation

In this chapter, all the thesis work are reviewed, and some possible future works are suggested.

6.1. Statics analysis by elements with rotational DOFs

From results of Chapter 3 show that introduce rotational DOFs will improve the performance of the elements. First, elements with rotational DOFs can produce accurate results in coarse mesh and converge faster than the element without rotational DOFs, Second, elements with rotational DOFs is insensitive to mesh distortion and high aspect ratio. Third, by comparing the results of bending behavior in these beam problem, it shows that element with rotational DOFs affected much less by shear locking.

6.2. Dynamics analysis by elements with rotational DOFs

From the results of chapter 4, it shows that dynamics analysis by elements with rotational DOFs can improve the accuracy of results, but the element with refined strain matrix may lead to poor results. First, the results of element AQ and element GQ12M with coarse mesh are close to the results computed by fine mesh, so the elements with rotational DOFs are performed better than the standard element. However, element QA4 produced poor results in dynamics analysis which is reasonable since its strain matrix is refined, but shape function remains unchanged. Thus, the stiffness matrix and the mass matrix will be mismatch, and lead to poor results.

6.3. Design optimization by elements with rotational DOFs

Results of design optimization by elements with rotational DOFs show performance improvement. From the sizing problem, elements with rotational DOFs can produce accurate results in the coarse mesh. Therefore, implementation of elements with

rotational DOFs will decrease the overall design optimization cost. For the topology optimization, the implementation of elements with rotational DOFs will prevent the checkerboard phenomenon. Therefore, the computing cost will decrease by removing the filter for checkerboard.

6.4. Possible future work

First, the rotational DOFs in those elements is not the true rotation defined in elasticity. Most vertex rotation in those elements is a rigid rotation. Therefore, introducing elasticity rotation to the element may be another way to improve element performance.

Second, the refined element performed poor in dynamics analysis compared to other elements with rotational DOFs. It is because the shape function was unchanged during the strain matrix refine process. This can happen on other refined elements. Therefore, it is expected to develop an approach to refine the shape function.

References

[1] D. Allman, "A compatible triangular element including vertex rotations for plane elasticity analysis," *Computers & Structures,* vol. 19, no. 1-2, pp. 1-8, 1 1 1984.

[2] P. Bergan and C. Felippa, "A triangular membrane element with rotational degrees of freedom," *Computer Methods in Applied Mechanics and Engineering,* vol. 50, no. 1, pp. 25-69, 1 7 1985.

[3] R. D. Cook, "On the allman triangle and a related quadrilateral element," *Computers & Structures,* vol. 22, no. 6, pp. 1065-1067, 1 1 1986.

[4] R. H. Macneal and R. L. Harder, "A refined four-noded membrane element with rotational degrees of freedom," *Computers & Structures,* vol. 28, no. 1, pp. 75-84, 1 1 1988.

[5] L. Yuqiu and X. Yin, "Generalized conforming triangular membrane element with vertex rigid rotational freedoms," *Finite Elements in Analysis and Design,* vol. 17, no. 4, pp. 259-271, 1 11 1994.

[6] D. J. Allman, "A quadrilateral finite element including vertex rotations for plane elasticity analysis," *International Journal for Numerical Methods in Engineering,* vol. 26, no. 3, pp. 717-730, 1 3 1988.

[7] Y. Long and Y. Xu, "Generalized conforming quadrilateral membrane element with vertex rigid rotational freedom," *Computers & Structures,* vol. 52, no. 4, pp. 749-755, 17 8 1994.

[8] W. Chen and Y. Li, "Refined non-conforming quadrilateral plane isoparametric element with drilling degrees of freedom," *computational structural mechanics and applications,* vol. 10, no. 1, pp. 22-29, February 1993.

[9] N. Stander and E. L. Wilson, "A 4-node quadrilateral membrane element with in-plane vertex rotations and modified reduced quadrature," *Engineering Computations,* vol. 6, no. 4, pp. 266-271, 11 4 1989.

[10] K. Sze, W. Chen and Y. Cheung, "An efficient quadrilateral plane element with drilling degrees of freedom using orthogonal stress modes," *Computers & Structures,* vol. 42, no. 5, pp. 695-705, 3 3 1992.

[11] R. D. Cook, "A plane hybrid element with rotational d.o.f. and adjustable stiffness," *International Journal for Numerical Methods in Engineering,* vol. 24, no. 8, pp. 1499-1508, 1 8 1987.

[12] S. M. Yunus, S. Saigal and R. D. Cook, "On improved hybrid finite elements with rotational degrees of freedom," *International Journal for Numerical Methods in Engineering,* vol. 28, no. 4, pp. 785-800, 1 4 1989.

[13] M. A. Aminpour, "An assumed-stress hybrid 4-node shell element with drilling degrees of freedom," *International Journal for Numerical Methods in Engineering,* vol. 33, no. 1, pp. 19-38, 15 1 1992.

[14] M. A. Aminpour, "Direct formulation of a hybrid 4-node shell element with drilling degrees of freedom," *International Journal for Numerical Methods in Engineering,* vol. 35, no. 5, pp. 997-1013, 30 9 1992.

[15] Y. S. Choo, N. Choi and B. Chai Lee, "Quadrilateral and triangular plane elements with rotational degrees of freedom based on the hybrid Trefftz method," *Finite Elements in Analysis and Design,* vol. 42, no. 11, pp. 1002-1008, 1 7 2006.

[16] X.-M. Chen, S. Cen, J.-Y. Sun and Y.-G. Li, "Four-Node Generalized Conforming Membrane Elements with Drilling DOFs Using Quadrilateral Area Coordinate Methods," *Mathematical Problems in Engineering,* vol. 2015, pp. 1-13, 19 5 2015.

[17] J. Simo, D. Fox and T. Hughes, "Formulations of finite elasticity with independent rotations," *Computer Methods in Applied Mechanics and Engineering,* vol. 95, no. 2, pp. 277-288, 1 3 1992.

[18] A. Cazzani and S. N. Atluri, "Four-noded mixed finite elements, using unsymmetric stresses, for linear analysis of membranes," *Computational Mechanics,* vol. 11, no. 4, pp. 229-251, 1993.

[19] R. H. Macneal and R. L. Harder, "A proposed standard set of problems to test finite element accuracy," *Finite Elements in Analysis and Design,* vol. 1, no. 1, pp. 3-20, 1 4 1985.

[20] R. D. Cook, "Improved Two-Dimensional Finite Element," *Journal of the Structural Division,* vol. 100, no. 9, pp. 1851-1863, 1974.

[21] Ü. H. Çalık Karaköse and H. Askes, "Static and dynamic convergence studies of a four-noded membrane finite element with rotational degrees of freedom based on displacement superposition," *International Journal for Numerical Methods in Biomedical Engineering,* vol. 26, no. 10, pp. 1263-1275, 17 12 2008.

[22] O. Sigmund, "A 99 line topology optimization code written in Matlab," *Structural and Multidisciplinary Optimization,* vol. 21, no. 2, pp. 120-127, 1 4 2001.

[23] B. Balogh and J. Lógó, "The application of drilling degree of freedom to checkerboards in structural topology optimization," *Advances in Engineering Software,* vol. 107, pp. 7-12, 1 5 2017.

[24] W. Zouari, F. Hammadi and R. Ayad, "Quadrilateral membrane finite elements with rotational DOFs for the analysis of geometrically linear and nonlinear plane problems," *Computers & Structures,* vol. 173, pp. 139-149, 1 9 2016.

[25] S. M. Yunus, "A study of different hybrid elements with and without rotational D.O.F. for plane stress/plane strain problems," *Computers & Structures,* vol. 30, no. 5, pp. 1127-1133, 1 1 1988.

[26] K. Wisniewski and E. Turska, "Enhanced Allman quadrilateral for finite drilling rotations," *Computer Methods in Applied Mechanics and Engineering,* vol. 195, no. 44-47, pp. 6086-6109, 15 9 2006.

[27] G. Pimpinelli, "An assumed strain quadrilateral element with drilling degrees of freedom," *Finite Elements in Analysis and Design,* vol. 41, no. 3, pp. 267-283, 1 12 2004.

[28] A. Madeo, G. Zagari and R. Casciaro, "An isostatic quadrilateral membrane finite element with drilling rotations and no spurious modes," *Finite Elements in Analysis and Design,* vol. 50, pp. 21-32, 1 3 2012.

[29] A. Madeo, R. Casciaro, G. Zagari, R. Zinno and G. Zucco, "A mixed isostatic 16 dof quadrilateral membrane element with drilling rotations, based on Airy stresses," *Finite Elements in Analysis and Design,* vol. 89, pp. 52-66, 15 10 2014.

[30] S. Kugler, P. A. Fotiu and J. Murin, "A highly efficient membrane finite element with drilling degrees of freedom," *Acta Mechanica,* vol. 213, no. 3-4, pp. 323-348, 11 9 2010.

[31] H. Kebari and A. C. Cassell, "Stabilization by non-conforming modes: 9-node membrane element with drilling freedom," *International Journal for Numerical Methods in Engineering,* vol. 31, no. 7, pp. 1453-1468, 20 5 1991.

[32] M. Iura and S. N. Atluri, "Formulation of a membrane finite element with drilling degrees of freedom," *Computational Mechanics,* vol. 9, no. 6, pp. 417-428, 1992.

[33] A. Ibrahimbegović, "Mixed finite element with drilling rotations for plane problems in finite elasticity," *Computer Methods in Applied Mechanics and Engineering,* vol. 107, no. 1-2, pp. 225-238, 1 8 1993.

[34] A. Ibrahimbegović and F. Frey, "Membrane quadrilateral finite elements with rotational degrees of freedom," *Engineering Fracture Mechanics,* vol. 43, no. 1, pp. 13-24, 1 9 1992.

[35] A. Ibrahimbegovic and E. L. Wilson, "A unified formulation for triangular and quadrilateral flat shell finite elements with six nodal degrees of freedom," *Communications in Applied Numerical Methods,* vol. 7, no. 1, pp. 1-9, 1 1 1991.

[36] A. Ibrahimbegovic, R. L. Taylor and E. L. Wilson, "A robust quadrilateral membrane finite element with drilling degrees of freedom," *International Journal for Numerical Methods in Engineering,* vol. 30, no. 3, pp. 445-457, 20 8 1990.

[37] A. Ibrahimbegovic, "A novel membrane finite element with an enhanced displacement interpolation," *Finite Elements in Analysis and Design,* vol. 7, no. 2, pp. 167-179, 1 11 1990.

[38] T. J. R. Hughes, A. Masud and I. Harari, "Dynamic analysis and drilling degrees of freedom," *International Journal for Numerical Methods in Engineering,* vol. 38, no. 19, pp. 3193-3210, 15 10 1995.

[39] A. A. Groenwold, Q. Xiao and N. Theron, "Accurate solution of traction free boundaries using hybrid stress membrane elements with drilling degrees of freedom," *Computers & Structures,* vol. 82, no. 23-26, pp. 2071-2081, 1 9 2004.

[40] S. Geyer and A. A. Groenwold, "Two hybrid stress membrane finite element families with drilling rotations," *International Journal for Numerical Methods in Engineering,* vol. 53, no. 3, pp. 583-601, 30 1 2002.

[41] D. Fox and J. Simo, "A drill rotation formulation for geometrically exact shells," *Computer Methods in Applied Mechanics and Engineering,* vol. 98, no. 3, pp. 329-343, 1 8 1992.

[42] R. D. Cook, "Some options for plane triangular elements with rotational degrees of freedom," *Finite Elements in Analysis and Design,* vol. 6, no. 3, pp. 245-249, 1 3 1990.

[43] R. D. Cook, "Modified formulations for nine-d.o.f. plane triangles that include vertex rotations," *International Journal for Numerical Methods in Engineering,* vol. 31, no. 5, pp. 825-835, 1 4 1991.

[44] N. Choi, Y. S. Choo and B. C. Lee, "A hybrid Trefftz plane elasticity element with drilling degrees of freedom," *Computer Methods in Applied Mechanics and Engineering,* vol. 195, no. 33-36, pp. 4095-4105, 1 7 2006.

[45] C.-K. Choi, T.-Y. Lee and K.-Y. Chung, "Direct modification for non-conforming elements with drilling DOF," *International Journal for Numerical Methods in Engineering,* vol. 55, no. 12, pp. 1463-1476, 30 12 2002.

[46] S. Cen, M.-J. Zhou and X.-R. Fu, "A 4-node hybrid stress-function (HS-F) plane element with drilling degrees of freedom less sensitive to severe mesh distortions," *Computers & Structures,* vol. 89, no. 5-6, pp. 517-528, 1 3 2011.

[47] A. A. Cannarozzi and M. Cannarozzi, "A displacement scheme with drilling degrees of freedom for plane elements," *International Journal for Numerical Methods in Engineering,* vol. 38, no. 20, pp. 3433-3452, 30 10 1995.

[48] D. Boutagouga, "A new enhanced assumed strain quadrilateral membrane element with drilling degree of freedom and modified shape functions," *International Journal for Numerical Methods in Engineering,* vol. 110, no. 6, pp. 573-600, 11 5 2017.

[49] D. J. Allman, "Evaluation of the constant strain triangle with drilling rotations," *International Journal for Numerical Methods in Engineering,* vol. 26, no. 12, pp. 2645-2655, 1 12 1988.

Appendix A

Matlab code structure

In this appendix, the main structure of the Matlab code used in this work will be introduced. The Matlab code is programmed through object-oriented programming techniques. These techniques allow organizing data and related functions simply.

The whole code is organized into five classes: *CStruct, CArea, CLine, CElement,* and *CPoint*. All the five classes are handle class so that the data modification in different functions will refer to the same object. All the data used in FEM computing will be stored in corresponding class and passed to the next class. In object-oriented programming, data stored in class is called property of the class, and the function stored in class is called method of the class.

A. Computing work flow

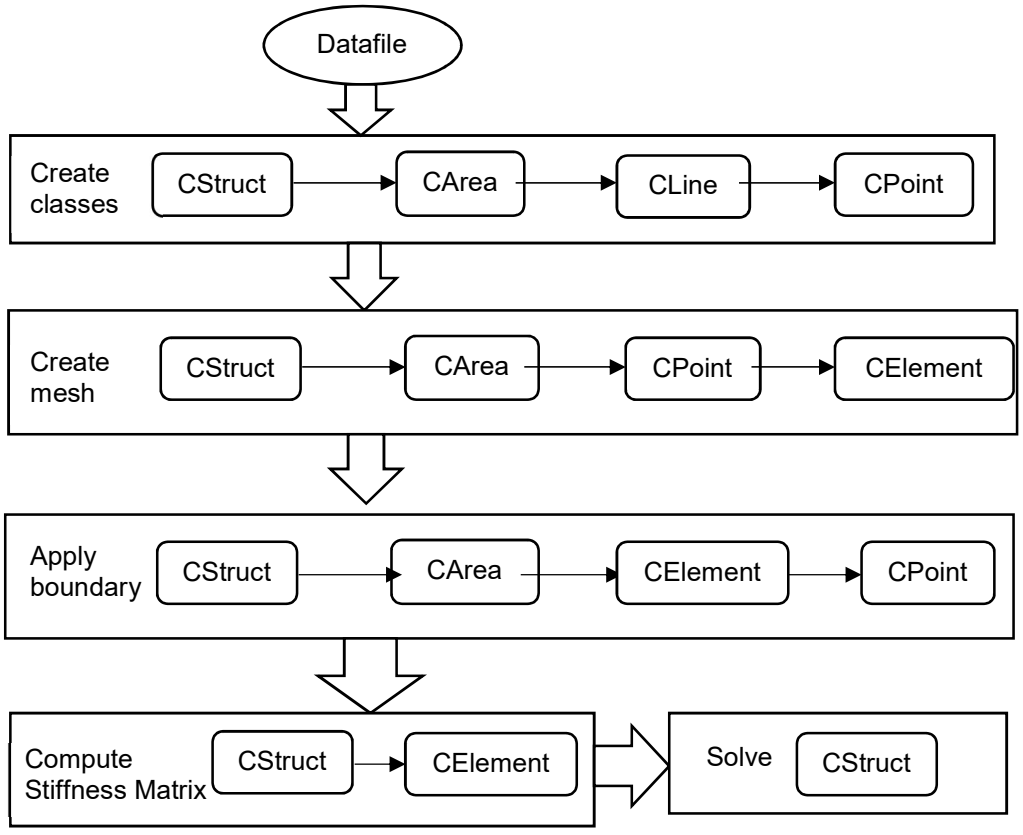

B. Classes properties and methods

(1) CStruct

The data and function related to the whole structure will be stored in this class. However, some global data will only be collected from sub-class and calculated when it is called and will be empty in other time.

Properties of CStruct:

Areas	Area Classes belong to this structure
DOF	Number of DOFs per node
DyUg	Global response for Dynamics
DyUi	Imaginary part of frequency response
DyUr	Real part of frequency response
ELEC	Points to form areas
ELHO	Areas with hole
ElementType	Element type
Elements	Element Classes belong to this structure
Freq	Frequency points for dynamics
Gauss	Default number of Gauss points
Lines	Line Classes belong to this structure
MTab	Table of material properties
NOAreas	Number of areas
NOElements	Number of elements
NOLines	Number of lines
NOPoints	Number of points
Name	Title of problem
Omega	Forcing frequency

Points	Point Classes belong to this structure
ProbeST	st-coordinates of probe points
ProbeXY	xy-coordinates of probe points
Time	Time points for dynamics
WN	Natural frequency
XY	xy-coordinates of key points
atype	Analysis type of dynamics
damp	Proportional damping coefficient
datafile	File which contain original data

Methods of CStruct:

CBC	Add boundary conditions
CEleType	Set element type
CLoad	Add boundary conditions
CMaterial	Add matrial properties
CMesh	Mesh Area
CProbe	Compute result at probe points
CSolve	Solve the FEM problem
CStiff	Compute stiffness matrix
CWeakSpring	Add weak spring if needed
OptUp	Update optimization design for topology
animation	Create animation for dynamic time response
find	Find the Probe Point location
plot	Plot the certain figure

(2) CArea

Properties of CArea:

Boundary	Boundary conditions of this Area
E	Young's Modulus for this Area
ElementList	Element Classes belong to this Area
ElementMatrix	Element Classes stored in matrix corresponding as mesh order
LineList	Line Classes belong to this Area
NO	NO. of this Area
PointList	Point Classes belong to this Area
PointMatrix	Point Classes stored in matrix corresponding as mesh order
rho	Density of this Area
thick	Thickness of this Area
v	Poisson's ratio of this Area
xelement	Number of element along x-direction
yelement	Number of element along y-direction

Method of CArea

CMaterial	Apply Material properties
CMesh	Mesh Area
CreateArea	Create Area
Fillin	Fill in Points for normal areas
GElem	Generate element for normal areas
GElemHO	Generate element for areas with hole
GMesh	Generate grid for normal areas
GMeshHO	Generate grid for areas with hole

(3) CLine

Properties of CLine

ElementList	Element on this line
NO	NO. of this Line
PointList	Point on this Line

Methods of CLine

CBC	Apply boundary conditions
CLoad	Apply line loads
Fillin	Fill in Points

(4) CElement

Properties of CElement

C	Damping matrix
E	Young's Modulus
ElementType	Element type
K	Stiffness matrix
M	Mass matrix
NO	NO. of this element
PointList	Point Classes belong to this Element
PointMatrix	Point Classes stored in matrix corresponding as place order
rho	Density
thick	Thickness
v	Poisson's ratio

Methods of CElement

CEleType	Assign element type
CLoad	Apply line load

CMaterial	Assign material properties
Cprobe	Compute result at probe points
animestrain	Compute strain for animation
animestress	Compute stress for animation
find	Find the Probe Point location

(5) CPoint

Properties of CPoint

BC	Boundary conditions
DOF	DOFs of this Point
Loads	Loading on this Point
NO	NO. of this point
U	Displacement of this Point
U0	Initial displacement
X	X coordinate
Y	Y coordinate
dU0	Initial velocity

Methods of CPoint

CBC	Apply boundary condition
CLoad	Apply loading
dist	Distence between two points